https://doi.org/10.5194/essd-2023-464
Preprint. Discussion started: 20 February 2024

Open Access Earth System Science Data Discussions

Integration by design: Driving mineral system knowledge using multi modal, collocated, scale-consistent characterization.

James R. Austin[1], Michael Gazley[2], Renee Birchall[2], Ben Patterson[1], Jessica Stromberg[2], Morgan Willams[2], Andreas Björk[1], Monica Le Gras[2], Tina D. Shelton[2], Courteney Dhnaram[3], Vladimir Lisitsin[3], Tobias Schlegel[2], Helen McFarlane[2], John Walshe[2].

[1] Potential Fields Geophysics, CSIRO Mineral Resources, West Lindfield, 2070, Australia
[2] Australian Resources Research Centre, CSIRO Mineral Resources, Kensington, 6151, Australia
[3] Mineral Systems Team, Geological Survey of Queensland, Brisbane, 4000, Australia

Correspondence to: Dr James R. Austin (james.austin@csiro.au)

Abstract. Recent decades have seen an exponential rise in the application of machine learning in geoscience. Fundamental differences distinguish geoscience data from most other data types. Geoscience datasets are typically multi-dimensional, and contain 1-D (drillholes), 2-D (maps or cross-sections), and 3-D volumetric and point data (models/voxels). Geoscience data quality is a product of its resolution and the precision of the methods used to acquire it. The dimensionality, resolution, and precision of each layer within a geoscience dataset translates to limitations in spatiality, scale and uncertainty of resulting interpretations. Historically, geoscience datasets were overlaid cartographically, to incorporate subjective, experience-driven knowledge, and variances in scale, and resolution. The nuances and limitations that underpin the reliability of automated interpretation are well understood by geoscientists, but are rarely appropriately transferred to data science. However, for true integration of geoscience data, such issues cannot be overlooked without consequence. To apply data analytics to complex geoscience data (e.g., hydrothermal mineral systems) effectively, methodologies must be used that characterise the system quantitatively, using collocated analyses, at a common scale. This paper provides research and exploration insights from an innovative district-wide, scale-integrated, geoscience data project, which analysed 1,590 samples from 23 mineral deposits and prospects across the Cloncurry District, Queensland, Australia. Ten different analytical techniques, including density, magnetic susceptibility, remanent magnetisation, anisotropy of magnetic susceptibility, radiometrics, conductivity, scanning electron microscopy (SEM)-based automated mineralogy, geochemistry, and short-wave infrared (SWIR) hyperspectral data with 561 columns of scale-integrated data (+2151 columns of SWIR). All data were collected on 2 cm x 2.5 cm sample cylinders; a scale at which the confidence in coupling of data from techniques can be high. These data are integrated by design, to eliminate the need to downscale coarser measurements via assumptions, inferences, inversions, and interpolations. This scale-consistent approach is critical to the quantitative characterisation of mineral systems and has numerous applications to mineral exploration, such as linking alteration paragenesis with structural controls and petrophysical zonation.

https://doi.org/10.5194/essd-2023-464
Preprint. Discussion started: 20 February 2024

Open Access Earth System Science Data Discussions

1 Introduction

With the increase in computer power and the algorithmic advances of the last decade(s), there is a new wave of statistical application to data analytics (Biamonte et al., 2017), with machine learning steadily gaining popularity since the turn of the millennium (Figure 1), proving effective for many applications (e.g., retail, finance). Not surprisingly, this new enthusiasm has spread to data-heavy fields of science, which has led to an exponential increase in the adaptation of machine learning to the analysis of geoscience data since 2010 (Figure 1). However, there are fundamental differences that distinguish geoscience data from most other data types to which machine-learning methods are commonly applied.

Geoscience datasets have highly variable precision across different data types and resolutions, which drastically effects the resolution at which datasets can be confidently correlated. They are intrinsically multiscale and are commonly analysed at different scales. In mineral exploration (for example) we often refer to regional, camp/deposit and sub-deposit scales (e.g., drillholes, individual samples: Figure 2). Scale in this sense may mean resolution (pixel) size of a 2-D image, the voxel size or the interpreted or interpolated 3-D volume (Figure 2) but can also refer to the volume on which an analysis is conducted from or area on which a measurement is made. This varies greatly across techniques from the km^3 to mm^3 scale. However, even in the context of geochemical data which is spatially simple point data (relative to the scale and depth complexities associated with geophysics), the volume/area of that point commonly varies from meters to centimetres, e.g., between a 1 m composite analyses and single-point portable X-ray fluorescence (pXRF) measurements. Complexities associated with the scale of different datasets may render data un-integrable even if they are collocated.

In addition to these scale issues, geoscience data are typically multi-dimensional, comprising 1-D information (e.g., drill holes), 2-D information in both map and cross-sections, and 3-D data (e.g., grids and voxels). For example, consider a demographics dataset which may be used to define where a new commercial service should be located. In these data, every piece of information is related to a single location (e.g., where a person lives) which has a unique spatial (X, Y) location. This is very similar to many geoscience datasets, for example in ground geochemistry; there may be several different parameters of the data for each point (e.g., Cu, Pb, etc); each point corresponds to a specific X, Y point on a surface. However, there is no tangible third dimension to this dataset, so it has no depth penetration, and the areal coverage of the data are infinitesimal in relation to the area of investigation (i.e., each point corresponds to a singular point, rather than describing a substantial 3-D volume. Interpreting such simple datasets is, not surprisingly, relatively simple even though one could use any manner of complex analysis. But, the addition of a 3-D component, as is common in many geoscience datasets, including the simple

https://doi.org/10.5194/essd-2023-464
Preprint. Discussion started: 20 February 2024

geochemistry example, but from drill core, adds another level of complexity, and with it, additional sparsity. This complexity of dimensionality interacts variably with scale complexity for different techniques.

Historically, geoscience datasets have been gathered incrementally, over long periods of time, by different people, for different purposes. Whilst different geological surveys and companies often have set methodologies for data collection, which no doubt evolve sporadically, there are no universally accepted ways of collecting analysing or even reporting geoscience data. Historically, geoscience data was designed for all manner of purposes, and collectively could be overlain in a manner more similar to cartography than true data integration. It can be more art than science to incorporate multiple datasets, with different scales, precision, depth of analysis. Geoscientists account for some of the differences in scale and resolution on the fly, but beyond that, may overlook that each layer corresponds to, and provides, completely different information. In a cartographic approach to data integration, overlooking the scale-resolution-dimensionality issue may not substantially affect the outcome. However, for true mathematical integration this issue cannot be overlooked without consequence.

There are many nuances, limitations, and pitfalls associated with most types of geoscience data that may significantly affect the outcomes of modern data-driven approaches. In many cases, these issues are well understood by domain experts, but this knowledge is often not appropriately transferred to data scientists. Some of the main issues may include:

1. An understanding of the effects of sample size, resolution, and dimensionality of different types of data, and the limitations thereof.
2. Recognition of the differences between various geophysical techniques, imaging, and point sample analysis (i.e., differences in intrinsic scale, depth of investigation).
3. Realisation that differences in the way data are processed, e.g., simple subjective interpretation, hand contouring, interpolation, and inversion, impact the precision of the resultant datasets.
4. Knowing that some datasets are partially complimentary in some instances (e.g., magnetics and gravity will often overlap), but most datasets are not complimentary at all, they describe unrelated properties, often at different scales and/or different crustal levels (e.g., geophysics).

Different approaches have been developed to overcome some of these issues over several decades. GoogleEarth™ imagery and associated 3-D city models (e.g., Gröger et al., 2005) use various functions to represent maps, and /or the 3-D buildings differently depending on the scale at which the user is zoomed in. This requires the database to have different resolution imagery and different scaled models available that can be loaded on the fly. Unfortunately, geoscience data tends not to be used in the same way. A common methodology for integrating potential field geophysics is to work within a voxel framework, and attribute petrophysical properties to voxels based on inversion of the data. Whilst convenient, such approaches may overlook issues of scale (e.g., gravity and magnetics data are integrated together even though there is a hundred-fold difference in their resolution), and ignore the issues of ambiguity, (e.g., especially that related to remanent magnetisation). If the resolution and depth sensitivities of the data used to derive 3-D volumes of the sub-surface vary substantially with our scale of investigation, so too should our models.

https://doi.org/10.5194/essd-2023-464
Preprint. Discussion started: 20 February 2024

A common way to use complex datasets in geoscience is to utilise statistical approaches (e.g., Allard et al., 2012) in which different sources of information are combined in a probabilistic framework. For example, in reservoir modelling, direct geological observations, geophysics, remote sensing, training images, etc., are used to determine the probability of occurrence of a certain lithofacies at a certain location. Such information can be readily computed based on certain conditions that are applied to the observed values in the source dataset. A strength of such approaches is their incorporation of uncertainty into the computational procedure. However, they sometimes fail to adequately account for the prediction uncertainty nuances of specific datasets (e.g., they may not effectively differentiate between different resolutions, penetration depths).

Volumetrically, once geoscience data are used to make predictions about 3-D geology, it must be accepted that there are far fewer knowns than unknowns. Much of our understanding is interpretation, not fact, and consequently, the uncertainty associated with each dataset, in the context of a large 3-D volume of rocks (e.g., the Cloncurry District) is very high. As we integrate more different types of data, the uncertainty propagates, and is often poorly captured in our models.

Rather than starting at the large scale, i.e., starting with a large area and attempting to force disparate datasets to describe concise voxels (3D pixels) in a model, it may be advantageous to work only at a scale at which we can be confident of the coupling of the datasets (i.e., at the small-scale). Using this approach, there is not the same ability to extrapolate the results across large areas or volumes mathematically. However, it is possible to measure all the possible parameters initially and at the same scale, to understand their relationships to one another. It is therefore a truly integrated dataset by design, which we do not need to integrate via questionable assumptions, inferences, inversions, and interpolations after the fact. Scale integrated, collocated dataset can be utilised, with confidence, for a variety of statistical and machine learning approaches, to understand the system holistically rather than integrating our data and ignoring all the aforementioned issues that effectively preclude the integration of many datasets. The outcomes from scale constrained analyses can be utilised to make better use of a suite of compatible but spatially distinct techniques at expanded scales, where their own specific nuances of scale, resolution and dimensionality, can be accommodated more effectively. For example, if a particular pattern that suggests mineralisation is related to a specific radiometric and magnetic signature, we can target such patterns in those specific regional datasets. As a by-product this approach provides ammunition to make better informed decisions about which datasets are crucial, and where individual dataset should be improved in terms of coverage, and/or resolution, and/or depth penetration and/or precision.

Here we present (to our knowledge) the world's first publicly available, district-wide, scale integrated, collocated, geoscience dataset. It incorporates 2712 columns of data (NB. >2000 of these are hyperspectral data), from 10 different techniques, and includes detailed petrophysical data, such as density, magnetic susceptibility, remanent magnetisation, magnetic fabrics (AMS), radiometrics, and conductivity. It contains comprehensive mineralogy and mineral texture and alteration information based on TIMA-SEM scans. Is also contains comprehensive geochemistry (from both portable XRF analyses and analyses of powders) and hyperspectral data. It contains information for 1,590 samples (many with three specimen each), extracted from 23 deposits and prospects: Altia, Artemis, Brumby, Barbara, Cameron River, Cannington, Canteen, Cormorant, E1 North, Eloise, Ernest Henry, Great Australia, Kalman, Kulthor, Little Eva, Maronan, Merlin, Monakoff, Mt Colin, Osborne, Starra-276, SWAN/Domain 81 and Trekelano.

https://doi.org/10.5194/essd-2023-464
Preprint. Discussion started: 20 February 2024

In geosciences, multiple techniques across a range of resolutions, spatial distributions, depth sensitivities and precisions, are used to vector toward mineralisation. This dataset allows all the major techniques used in mineral exploration to be correlated and contrasted at the same scale by providing quantitative, integrated insights into the processes that control geophysical signatures and better inform our understanding of the relationships between alteration and structure. This dataset is integrated by design, and is "complex" data (many columns), not "big" data (many rows). But, if used to its full potential, it enables more effective translation of geochemical, structural, and geological processes into the physical parameters required to make big data tangible in the mining space. It can shift the current paradigm in mineral exploration (i.e., using a mixture of qualitative and quantitative data at different scales), toward the fully quantitative, scale-consistent datasets required to make big data tangible in the mineral system space. We hope that this dataset it will lead to new discoveries that are so vital to the economy of the Mount Isa region, Australia, and furthermore hope it provides the impetus and inspiration for re-thinking the role of data in the outcome of data analytics.

2 **Study Area**

The Cloncurry District (Figure 3) is a richly endowed region in Queensland, Australia, that contains a range of mineral systems which produced deposits of various commodities, including base metals, precious metals, and rare earth elements. It has undergone a protracted structural and metasomatic history (e.g., Rubenach, 2013). Whilst there is much conjecture as to the genesis of deposits and timing of different styles of mineralisation (e.g., Groves et al., 2010; Hitzman et al., 1992; Hitzman and Porter, 2000; Williams et al., 2005), there is general agreement on the broad timing of major structural, metamorphic, magmatic, metasomatic and mineralisation events (Figure 4).

The Cloncurry district is very diverse in terms of the types and styles of mineralisation present. It is famous as an iron oxide copper-gold (IOCG) district, but in many ways, there are few *sensu stricto* IOCG deposits present (e.g., Ernest Henry, SWAN, E1 North) based on earliest classifications (e.g., Hitzman, et al., 1992). Many deposits could be referred to as IOCG-related (e.g., Monakoff, Starra, Osborne), but Broken Hill Type (BHT), skarn, and volcanogenic massive sulphide (VMS) types are also present. Various studies have recognised a continuum between different mineralisation styles in different deposits (e.g., Williams, 1998; Austin and Blenkinsop, 2009; Little, 2019), and the Cloncurry deposits contain mixtures of iron-apatite (Kiruna style), magnetite-dominant IOCG, pyrrhotite-dominant iron sulphide copper-gold (ISCG), and hematite-dominant IOCG assemblages. There is also an array of skarn-like assemblages (Williams and Heinemann, 1993; Williams and Baker, 1995; Roache, T. J., et al., 2005). These include dolomite-magnetite-chalcopyrite (e.g., Starra-276; Patterson et al., 2016), to calcite-pyrrhotite-sphalerite-chalcopyrite assemblages (e.g., Artemis: Austin et al., 2016a; Knorsch et al., 2020), calcite-pyrrhotite-chalcopyrite assemblages (e.g., Canteen; Austin et al., 2016b), calcite-pyrrhotite-galena (Maronan; Austin et al., 2016c), calcite-barite-fluorite-magnetite-chalcopyrite (e.g., Monakoff; Austin et al., 2016d). There is also a range of high temperature garnet, pyroxene and amphibole-rich (i.e., non-carbonate) 'skarn-like' varieties present, predominantly in the more Pb-Zn rich mineralisation types including Cannington (Chapman and Williams, 1998; Roach et al., 2005), Pegmont (Williams

https://doi.org/10.5194/essd-2023-464
Preprint. Discussion started: 20 February 2024


Open Access Earth System Science Data Discussions

et al, 1998), Maramungee (Williams and Heinmann, 1993) and Maronan (De Jong, 1995; Austin et al., 2016c). Austin and Blenkinsop (2009) suggested some of these deposits have characteristics which are transitional with those generally considered part of VMS (e.g., Maronan: Austin et al., 2016c) and/ or IOCG style systems (e.g., Monakoff: Austin et al., 2016d).

The Cloncurry District is geochemically, structurally, geophysically and metallogenically complex. It has long been a challenging terrane for explorers, and many, often conflicting interpretations have been generated for the district over the last century. Much of our knowledge of the district is qualitative, not quantitative. The district is globally unique in the diversity of mineralisation styles, related alteration assemblages, structural controls and geophysical signatures. Whilst it is tempting to pigeonhole different styles of mineralisation within the system, researchers are starting to recognise that perhaps these seemingly disparate mineral deposits are part of a larger interrelated system. The dataset that presented here, provides a unique opportunity to examine this complex mineral system through quantitative and scale-consistent means. We believe that this style of dataset is a pre-requisite to gain useful quantitative insights into the Cloncurry District, which will, hopefully, lead to some step changes in how we explore in this highly complex piece of the Earth's crust.

2 Sampling

2.1 Sampling Strategy

The aim of this project was to develop a comprehensive sample suite which is representative of the deposits and prospects in the region, with particular focus on the significant resources contained in the Ernest Henry, Starra-276, Osborne, SWAN, Eloise and Cannington deposits. Systematic sampling is critical for maximising exploration insights into the system, and furthermore providing data that can be used to understand zonation in the system. To achieve that, several basic criteria were used in selecting drillholes from each mineral system to sample.

2.1.1 Drillhole Selection

Drillholes were selected to gain a representative cross-section across the mineral system from distal country rock through to the orebody. When possible, drill hole selection and sampling was undertaken on site in collaboration with our industry partners who were intimately familiar with the mineral system to be sampled. However, in many cases, drillhole selection was limited by access and stakeholder priorities, and in many cases samples were selected from a list of holes available at the Geological Survey of Queensland (GSQ) drill core library.

2.1.2 Zonation

The aim of the drill hole selection and sampling was to provide a representative, scale –consistent, sample suite across each mineral system. Sampling was conducted from hanging wall to footwall, and ore, to proximal, medial and distal alteration, through to background in each deposit or prospect. This is relatively straightforward for upright linear systems with clearly defined foot and hanging walls such as Starra-276 (Section 2.2.4). However, there are many types of systems with different

https://doi.org/10.5194/essd-2023-464
Preprint. Discussion started: 20 February 2024

styles of zonation. Breccia pipes, for example, may have concentric zonation, and Broken Hill Type systems may have elements of stratiform zonation and fault-controlled replacement. Sampling from surface to depth was particularly important for systems modified by near surface (e.g., supergene) alteration (e.g., Starra-276, E1-North). Good coverage across strike and along strike was sought, where possible, and consistent areal coverage when sampling in an open pit, e.g., Osborne. However, in many cases it was not possible to achieve consistent areal coverage. In a mine setting this was due to several reasons including exposed underground workings, collapsed mine walls or unsafe wall conditions. Surface sampling also presented challenges where only competent units outcrop at surface (e.g., silicified ironstones at Starra-276), and adjacent recessive units are not exposed or too weathered for sampling.

2.1.3 Sample Spacing

Representative sample spacing down hole throughout a mineral system is critical to ensure a representative view of the 3-D volume of the system is captured in the dataset. However, this is almost never possible due to a range of factors. Inhibiting factors for drillcore sampling include variability in the quality of core (e.g., due to weathering, shearing, cracking), unsuitable sample volumes, mainly as a result of assaying (e.g., different core sizes and with full, ½ or ¼ core), and whether individual lengths of core were oriented. Sample frequency for surface sampling is mainly limited by where fresh rocks crop out, and mine sampling is mainly limited by the location of mine walls and safety factors. Furthermore, zonation in mineral deposits and their alteration halos can be very different, ranging from < 1 meter to kilometres in scale, and some sampled drill holes were on the scale of >500 m. And so, for practical reasons, sampling frequency was varied depending on the complexity of the system locally to capture a representative suite of samples. In complex and heterogenous lithologies, sampling frequency was higher (e.g., <1 m in mineralised zone), whereas in more homogenous and distal lithologies, sampling frequency was typically reduced (e.g., >10 m).

2.1.4 Representativity

Samples were selected to be representative of the lithology of that part of the hole (i.e., similar to the majority of the core across several trays) in order to capture the bulk physical properties of that lithology. Adopting this strategy allows for up-scaling of the physical properties with some confidence for use in geophysical modelling. Whilst some of the sampling conducted adheres to this methodology quite stringently, there are many cases of: oversampling through the mineralised zones, under-sampling through the mineralised zones where no core remained in the tray, and cases where samples could not be obtained due to lack of appropriately sized or appropriately oriented core. Sampling frequency was higher in mineralised intersections, moderate in the footprint, and relatively sparse in distal-background host rocks.

2.1.5 Orientation

Oriented samples are critical for geographic corrections to both anisotropy of magnetic susceptibility (AMS) and also remanent magnetisation measurements. In some cases, where holes are drilled at near vertical orientation, caution should be taken in

https://doi.org/10.5194/essd-2023-464
Preprint. Discussion started: 20 February 2024

interpreting AMS and palaeomagnetic results, because where dip approaches 90˚, orientation data becomes increasingly unreliable. However, in general, holes will tend to lift with depth, and as the plunge decreases, the orientation becomes increasingly reliable (even at orientations of ~85˚).

2.2 Sample Distribution

The data here presented were gathered from 1,590 samples, taken from 23 mineral deposits and prospects across the Cloncurry District, Queensland. The sampling was undertaken on several pilot projects from 2011– 2014 and two major Queensland Government Funded projects; Uncover Cloncurry 2015–2016, and Cloncurry METAL (2018–2021).

2.2.1 Uncover Cloncurry Samples

The Uncover Cloncurry project collected relatively few samples per deposit, but provides a broad overview of the different styles of mineralisation present in the Cloncurry District, and the Cloncurry Mineral System as a whole. Deposits and prospect types sampled include Broken Hill Type (BHT) deposits, such as Altia Pb-Zn-Ag, Artemis Zn-Cu, Maronan Pb-Zn-Ag, Iron Oxide Copper-Gold type, including Brumby Cu-Au, E1 Cu-Au, Kalman Cu-Au-Mo, Monakoff Cu-Au, Trekelano Cu-Au and related breccia sulphide ores (e.g., Merlin Mo-REE), Iron Sulphide Copper-Gold (ISCG) type, including Canteen Cu-Au, Cormorant Cu-Au, and skarns (e.g., Mount Colin). Sampling was undertaken on only one or two diamond drill holes for many of these deposits and prospects, and in these cases, the sampling cannot be considered representative. However, in other cases (e.g., Maronan, Brumby) a significant number of diamond drill hole samples and in some cases blocks and hand-drilled samples were extracted from mine pit walls (e.g., Monakoff, E1). Information on the location and geological context of those samples can be found in the Uncover Cloncurry reports, e.g., Austin et al., (2016 a-h), Gazley et al., (2016a, 2017) and Patterson et al., (2016a-b) or discussed further below.

2.2.2 Ernest Henry Cu-Au Deposit

Ernest Henry is the most comprehensively sampled deposit in this dataset, with samples from ten diamond drill holes. The bulk of the holes intersect the core of the deposit (e.g., EH691, EH550 and EH435), with representative holes intersecting the proximal (e.g., EH631), medial (e.g., EH632) and distal (e.g., EHMT001) parts of the alteration footprints across strike to the southeast. Other holes are intended to sample the proximal (e.g., EH147), medial (e.g., EH 242) and distal zones (e.g., MMA002 and MMA003) along strike to the northeast of the deposit. Sampling for Ernest Henry was completed in four different phases. Initial sampling of EH691 was completed onsite at the Ernest Henry Mine. Phases 2–4 were completed as drill holes were made available at the GSQ core facility in Zillmere, Queensland, Australia. A summary of the drill holes sampled is provided in Figure 5, and a detailed descriptions of the samples and the context within the deposit and its environs are provided in Schlegel et al. (2021, 2022); Austin and McFarlane (2021) and Austin et al. (2021).

https://doi.org/10.5194/essd-2023-464
Preprint. Discussion started: 20 February 2024


Open Access Earth System Science Data Discussions

2.2.3 Osborne Cu-Au Deposit

Osborne was sampled both from drill core and surface, in which the two sampled drill holes (OSHQ0067 and TTNQ0364, total of 42 samples) cut across the mineralised zone in the near-surface and towards the base of the mineral resource (Gazley et al., 2016b) (Figure 6). Surface samples were taken largely due to the lack of availability of fresh drill core in 2018-2020. Samples were collected from several traverses across key sections of the open pit, providing excellent coverage (52 hand-drilled cores and oriented block samples) of the deposit particularly the lower and upper ironstone horizons (Figure 7). Numerous samples were also taken outside the mineralised horizons. However, it was not possible to undertake a representative sampling grid due to several factors including ground instability (i.e., the large debris slope in the middle of the mine), which contributed to the lack of samples between the two main ironstone horizons. Other complicating factors included risks associated with working under high/steep pit walls, and restricted access to areas in which underground workings were exposed. All the samples were accurately surveyed courtesy of Chinova mine surveyor, and further information on samples and their context within the deposit and its environs are provided in McFarlane et al. (2021a).

2.2.4 Starra-276 Au-Cu Deposit

Starra-276 was also sampled in drill core and at surface and was intended as a case study for collection of surface samples. However, the local outcrop is so dominated by highly competent (silicified) hematite-ironstones that very few other samples could be obtained from the incompetent, weathered and eroded units on either side. This resulted in 27 hand-drilled and block samples from the surface at Starra-276 (Figure 8), most of which are ironstones, cropping out above and to the north and south of Starra-276. These were collected to assess along-strike geochemical variability in the ironstones, and for comparison with samples from depth to test the vertical zonation within the system (e.g., supergene enrichment). The remaining samples are from three diamond drill holes which form an E-W cross-section through the system with 38 samples from STQ1095 and 61 drill core samples from two scissor holes covering both the foot and hanging wall of the Starra-276 mineral deposit (Figure 9). Whilst on-site, detailed magnetic susceptibility logs for the scissored drill holes were acquired, which can be used for comparison with geochemical data. Further information on sampling and their context within the deposit and its environs are provided in McFarlane et al. (2021b).

2.2.5 Cannington Ag-Zn-Pb Deposit

Ten drill holes were sampled at the Cannington Mine site, aiming to cover the deposit from north to south and shallow to deep (Figure 10). The 190 samples collected provide a representative array of the seven different styles of mineralisation found at Cannington, i.e., the Kheri, Cuckadoo, Broadlands, Glenholme, Burnham, Inveravon, and Nittsdale types, and a representative selection of the host rocks of the deposit in both the northern and southern zones. Samples were taken from outside the system into the core mineralisation types to assess the proximal to distal footprint of the system. Although there are uncertainties as to the extent of the footprint of the Cannington deposit (many suggest a small alteration footprint), we aimed to get a

https://doi.org/10.5194/essd-2023-464
Preprint. Discussion started: 20 February 2024

representative selection of what the local geologists interpret as the footprint, referred to as SHMU (sillimanite-muscovite shist). Drill hole CAD934, which skims the body sampling the periphery of the system from shallow levels to depth under the body, provides an opportunity to test the extent of the deposit footprint. Further information on sampling and their context within the deposit and its environs are provided in Pearce et al. (2021).

2.2.6 SWAN Cu-Au Deposit

The SWAN-Mt-Elliot core system was sampled from 4 drill cores, three from the SWAN system, and one from Mt. Elliot ~900 m to the east. MEQ1215 (56 samples) was drilled into the hanging-wall of the SWAN system, dipping to the southwest through the main ore/breccia body. Additional holes were selected to generate a representative E-W cross section through the SWAN system, intersecting the distal and proximal alteration zones, through the main ore/breccia body (Figure 11). Drillholes MEHQ07105 (8 samples) and MEHQ011130 (52 samples) are to the east of MEQ1215 and are scissored holes which cut through the main breccia body from the east and west respectively. MEQ-95-208 is sampled from ~195 m depth in the Mount Elliot hanging, through a 'skarnoid' mineralised zone and into the footwall. Further information on sampling and their context within the deposit and its environs are provided in Stromberg et al., (2021) and Patterson et al., 2016.

2.2.7 Eloise Au-Cu Deposit

Eloise was sampled from drill core (58 samples) with a focus on Eloise Deeps and three satellite deposits. This included intervals from Eloise Deeps drill holes ED62 and ED60, and sampling of Macy (MA03E), Chloe (EN003) and Middle West (EAM130) (Figure 12). In addition to the intervals sampled in ED62 and ED60, a deep drill hole through the main orebody at Eloise Deeps was systematically sampled (ED126). The samples selected at each of the four mineralised bodies are representative of the deposit's stratigraphy and the sampling attempted to capture any proximal to distal footprints associated with mineralisation as well as intersect the various lodes, with an average sample interval of 30 m. Further information on sampling and their context within the deposit and its environs are provided in Birchall et al., 2021.

3 Methods

3.1 Sample Preparation

The samples were extracted from surface and mine sampling (Starra-276, Osborne, Monakoff, E1) and diamond drill holes as outlined in section 2. The physical samples include:

1. Twenty five mm diameter cores, drilled in situ with a petrol-powered rock drill. These samples were oriented in situ using a sun compass which is unaffected by extreme local magnetic fields present at many sites. These samples in some cases need to be re-assembled and glued, before being marked with orientation lines, sample numbers and cut into specimens.

https://doi.org/10.5194/essd-2023-464
Preprint. Discussion started: 20 February 2024

2. 10-30 cm blocks extracted with cold chisel and hammer from the surface outcrops and open pits. These samples were also oriented using a sun compass in the field. The sun compass orientation marks are used to draw azimuth lines on the block, which is then redrilled perpendicular to the orientation surface, thus transferring the orientation mark from block to cylinder.
3. 10-30 cm pieces of either ½ NQ or ¼ HQ core sampled from diamond drill holes. The orientation method for diamond core differs from the standard palaeomagnetic method, with marks pointing downward along the base of the hole (Figure 13a). Therefore, orientations were re-marked to the standard palaeomagnetic system prior to re-drilling and cutting (Figure 13). In this system: Palaeomagnetic Azimuth = Diamond drill dip azimuth - 90˚; Palaeomagnetic dip = 90˚ - Diamond drill plunge Drill core was marked-up in the standard palaeomagnetic method (Figure 13b). The resultant azimuth and dip correspond to a plane normal to the drill hole. A 25 mm diamond core drill was used to drill down the axis of each sample.

The 25 mm cores were sawn into 22 mm long segments referred to as 'rounds' (Figure 13c). Cylinders of this dimension provide a good approximation of a dipole magnetic source (Riisager & Abrahamsen, 2003). At least three rounds were made from each sample where possible, to provide statistically reasonable mean values for the petrophysical measurements. Preparing three samples also allowed for one sample to be used for geochemistry and mineralogy and one for Alternating Field Demagnetisation (AFD), with one reserved for other analyses. Samples were labelled and marked up with orientation lines (Figure 13c), to extract vector information from the samples, e.g., palaeomagnetic vectors and magnetic fabrics (i.e., anisotropy of magnetic susceptibility; AMS).

3.2 Techniques (methods, instrumentation, data processing and pitfalls)

3.2.1 Density Measurements

Density calculations were made based on mass measurements made using a Mettler Toledo MS204TS analytical balance. However, for legacy samples, other instruments may have been utilised (see column U in the database). The Archimedes principle was used to calculate the density of each sample. Samples were initially weighed in air and then subsequently weighed in distilled water. The density and volume of each sample was calculated using the following equations:

$$\text{Eq. (1)} \quad \rho = \frac{A \times \rho L}{A - B} \qquad \text{Eq. (2)} \quad V = \frac{A}{\rho}$$

Where ρ = density, A = sample weight in air, B = sample weight in liquid, ρL = density of the liquid, and V = sample volume. Volume results determined in these calculations are used for volume corrections for various other petrophysical parameters, specifically magnetic susceptibility and NRM measurements.

Density was determined for up to three specimens for each sample (columns P-R in the database) to derive a mean density value (column S) for the sample and an associated standard deviation (column T).

https://doi.org/10.5194/essd-2023-464
Preprint. Discussion started: 20 February 2024

3.2.2 Magnetic Susceptibility Measurements

Magnetic Susceptibility measurements are the most common type of petrophysical quantity collected in mineral exploration, and along with measurements of remanent magnetisation allow determination of the in-situ magnetisation of different lithologies and alteration styles, that can be used to constrain forward modelling and inversion. Magnetic susceptibility measurements were made using an Agico MFK1-A Kappabridge magnetometer. However, for legacy samples, other instruments may have been utilised (see column AA in the database).

The MFK1 Kappabridge apparatus consists of the Pick-Up Unit, Control Unit and Computer, and represents a precision fully automatic inductivity bridge. It automatically zeros between readings and automatic compensates for the thermal drift of the bridge and automatically switches to appropriate range. The measuring coils are designed as 6th-order compensated solenoids with a high field homogeneity. The instrument is based on micro-electronic components, with two microprocessors controlling all functions of the Kappabridge, and is fully controlled by an external laptop computer. The output signal from pick-up coils is amplified, filtered and digitalized, and raw data are transferred directly to the computer in the form of .RAN files and or .AMS files, which are native formats for AGICO's Anisoft™ 4.2 and 5.0 software packages.

Bulk susceptibility measurements were taken with the field strength set at 200 A/m to maximise the dynamic range of the sensor. The MFK1-A calculates magnetic susceptibility values based on a nominal sample volume of 10 cm^3 and as such, the results were later corrected using volumes calculated during density measurements. Users should be aware that the instrument can realistically only measure 10 cm^3 samples up to susceptibilities up to ~2.25 SI. In some cases, particularly in magnetite-rich or mushketovite-rich ironstones, susceptibilities are likely much higher, probably in the range of 10-20 SI (Clark, 1988). Magnetic susceptibility measurements were made on up to three specimens for each sample (columns V-X in the database) to derive a mean magnetic susceptibility value (column Y) for the sample and an associated standard deviation (column Z). Magnetic susceptibility is commonly plotted relative to density to compare the properties of different deposit types, and their alteration haloes, e.g., Figure 14.

3.2.3 Remanent Magnetisation Measurements

The direction of remanent magnetism is important in understanding the overall magnetization strength and direction in highly magnetised mineralised bodies (e.g., Peculiar Knob; Schmidt et al., 2007). Understanding remanent magnetism is crucial to determining confidence in the resultant 3-D model because it facilitates a reliable estimation of the impact of remanent magnetization on the overall (i.e., induced + remanent) magnetization of the prospect. Where magnetised rocks have a high Koenigsberger ratio (high ratio of remanent to induced magnetization), and where the remanent magnetisation direction is significantly oblique to the inducing field, anomalies will be incorrectly modelled if they do not account for the remanent magnetisation.

At least two rounds from each sample underwent natural remanent magnetisation (NRM) measurements. The process requires the input of the sample orientation data to correct the measured magnetisation direction to geographic coordinates. For the

https://doi.org/10.5194/essd-2023-464
Preprint. Discussion started: 20 February 2024

Cloncurry METAL project, all samples were measured using an AGICO JR-6 spinner magnetometer. However, many of the legacy samples which are included in the Cloncurry METAL database (Austin et al., 2021d) have been measured on a 2G Enterprises 755R three-axis cryogenic magnetometer and/or a custom-made CSIRO three-axis spinner fluxgate magnetometer.

The JR-6 spinner magnetometer is the world's most sensitive and accurate instrument for measurement of remanent magnetization of rocks based on classical (non-cryogenic) principle and is the standard for palaeomagnetism world-wide (AGICO, 2021). It functions by rotating the rock specimen at a constant angular speed inside the Pick-Up Unit inside a pair of coils. An alternating current (AC) voltage is induced in the coils whose amplitude and phase depend on the magnitude and direction of the remanent magnetization (RM) vector of the specimen. The resultant voltage is amplified, filtered and digitized. Using harmonic analysis, the computer calculates two rectangular components of the projection of RM vector into the plane perpendicular to the axis of rotation. The JR-6A version used, has an automatic specimen holder which changes the position of the specimen during measurement to get the complete vector automatically. The measurement process is fully controlled by a PC notebook or desktop and the data are interpreted using AGICO's Rema software.

The 2G cryogenic magnetometer uses three superconducting-quantum-interference-devices (SQUIDS) to measure the three components of the magnetic field with magnetic dipole moment noise of less than 1 x 10^{-12} A/m. Unfortunately, this system does not have the dynamic range necessary to measure strongly magnetised specimens. Strongly magnetised specimens therefore had to be measured on the 3-axis spinner magnetometer. The 3-axis spinner utilises a fluxgate magnetometer positioned adjacent to the sample spinning mechanism. The results of the NRM measurements yielded a magnitude, declination, and inclination of the magnetisation direction. The data extracted from the 2G and custom spinner magnetometers is comprised of simple ASCII file which require substantial re-formatting before interpretation using Pmag software developed by Phil Schmidt (CSIRO). Remanent magnetisation and or Koenigsberger ratio (J:K) are commonly plotted relative to density (Figure 15) and/or magnetic susceptibility to characterise the dominant magnetic minerals (e.g., Hematite, magnetite and pyrrhotite) within deposits and their footprints which generally form under different redox conditions.

3.2.4 Conductivity

Minerals act as semiconductors or insulators (silicates and oxides) in crustal rocks. In metal exploration, unlike fluid-saturated rocks in petroleum petrophysics, conductivity is not primarily related to ions in pore fluids. Instead, conductivity is heavily dependent on the presence and interconnectivity (fabric) of metal-bearing minerals, especially chalcopyrite and galena.

Conductivity measurements were carried out up to three rounds per sample. A KT-20 Handheld Susceptibility and Conductivity Meter was set to 100 kHz which provided a sensitivity as low as 0.1 S/m. The equipment is widely used in the industry for susceptibility measurements but is prone to providing ambiguous results. A custom-made holder was utilised to counter ambiguity caused by the operator. This ensured the measurements always had the flat end of the round centred on the sensor. The results were viewed directly on the instrument display and imported into the accompanying GeoView program. Subsequently, they were exported as discrete records in .CSV format, which were collated for the database by .BAT script and then cross-checked against a measurement log. Users of this data should be aware that electrical resistivity and conductivity

https://doi.org/10.5194/essd-2023-464
Preprint. Discussion started: 20 February 2024

measurements are highly scale-dependent (Fitzpatrick, 2006). Fitzpatrick (2006) suggests conductivity should be measured on 1 m diamond core to get reliable results. Whilst conductivity is measured at a consistent scale across all samples, the sample size is sub-optimal, and our conductivity measurements should be considered useful estimations of where sulphide occurs. Chargeability is not scale dependent and would be a more suitable data to collect on small cores such as those used in this study.

3.2.5 Radiometrics

Radioactive isotopes have played an important role as a heat source during the Earth's history, and heat generation from intrusions is often included in geological models. The overall radioactivity is known to have been higher at the time of the formation of the Cloncurry METAL project deposits. Relevant for heat production in these rocks are the radioactive isotopes of Uranium (238U), Thorium (232Th) and Potassium (40K). The heat generated per second by these elements (µWkg-1) would be presented as concentrations cU, cTh, and cK, respectively, the total Qr is the heat produced by radioactivity in the rock (Rybach, 1976, 1988):

Eq. (3) $Q_r = 95.2cU + 25.6cTh + 0.00348cK$

Radiometric measurements were conducted with a Radiation Solutions RS-332 Gamma-Ray Spectrometer and a custom-made tray holding up to three rounds per measurement. For most samples, all three slots were used for Assay Mode measurements. The accompanying RS Analyst program was used to catalogue and export of the data. Results were tabulated with K (Potassium-40), U (Uranium/Radium), Th (Thorium-232), Dose and Dose rate, using respective data units (%, ppm, µSv etc). The data was imported into the database together with the measurement ID, a note on the number of rounds in each of the measurements. Standard radiometric ratios, K:U, K:Th, U:Th, Th/K, U/K, U^2/K were calculated and also listed in the database. These ratios are a means of normalising the relative proportions of K, Th and U in different rock types, independent of their total count, to differentiate K, Th and U anomalism. It has long been recognised that Uranium anomalism in airborne radiometric data correlates with mineralisation and fluid pathways at numerous sites within the study area (Lambourn and Shelley, 1972). However, gamma-ray spectrometry at the sample scale provides a petrophysical means of integrating mineralogical and geochemical understanding of ore formation providing knowledge that can be used to better interrogate airborne radiometric datasets (e.g., Austin et al., 2021 d, Austin, 2021b). Uranium anomalous specimen (i.e., those with U^2:K > 10 in Figure 16) have distinct mineralogical properties. They all occur in IOCG or ISCG deposits and prospects and contain carbonates (either calcite and/or dolomite) and apatite. They are mineralogically complex and preserve mixed feldspar, titanium and iron oxide and iron sulphide assemblages (e.g., contain both magnetite and pyrrhotite, magnetite and hematite, and/or titanite ± rutile and ilmenite). Walshe et al. (2016) has argued that the distribution of andesine-ilmenite assemblages versus K-feldspar-titanite assemblages can be used to define pH and/or redox gradients in IOCG systems.

https://doi.org/10.5194/essd-2023-464
Preprint. Discussion started: 20 February 2024

3.2.6 Structural Fabrics

Methods

Anisotropy of magnetic susceptibility (AMS) is a second-order symmetric tensor that maps alignment of iron in the crystal lattice (Biedermann, et al., 2015) and therefore maps mineral alignment in rocks (Figure 17). AMS is often used as a proxy for mineral texture in geologic applications (Biedermann, et al., 2015). AMS fabrics have been related to numerous events through a range of temperature-pressure conditions, from viscous flow in magmas (e.g., Knight and Walker, 1988; Ferré et al. 2002) through to folding and ductile-brittle shearing during relatively late stages of orogenesis (e.g., Torsvik et al., 1992; Greiling and Verma, 2001, Austin et al., 2019b).

Anisotropy of magnetic susceptibility (AMS) measurements were made on most samples using an AGICO MFK1-A Kappabridge magnetometer. The MFK1-A effectively measures the axes of maximum, intermediate, and minimum susceptibility and relates those to the fabric of the magnetic grains with the rock.

For legacy samples (Uncover Cloncurry), 64 measurements are taken while spinning the specimen about the X, Y, and Z axes individually, using a conventional single axis rotator attachment. The field sensor is zeroed after the sample is inserted into the pick-up coil thereby eliminating any field bias from the measurements made as the sample is rotated. Then one bulk susceptibility value is measured along one axis and the complete susceptibility tensor is combined from these measurements. For Cloncurry METAL measurements, a 3D-rotator attachment was used. The 3D-rotator spins the specimen simultaneously about two axes with different velocities enabling the determination of 320 directional susceptibilities during a single measurement phase (constituting an excellent 3-D distribution within a sphere). Once the specimen is inserted into the rotator, measurement is fully automated, requiring no additional manipulation to measure the full AMS tensor, and halving the time for measurement. The output signal from pick-up coils is amplified, filtered, and digitalized, and raw data are transferred directly to the computer in the form of .RAN files and or .AMS files, which are native formats for AGICO's Anisoft 4.2 and 5.0 software packages (Chadima and Jelinek, 2009), either of which can be used to view and analyse the data.

Data

The AMS data are displayed for each specimen separately in the database: Specimen A: columns CG-DC; Specimen B: columns DD-DZ; Specimen C: columns DD-DZ. The resulting data are comprised of a bulk susceptibility (column CH in the case of Spec A) and three orthogonal tensors that together define the AMS ellipsoid. The three tensors are the long-axis (K1), an intermediate-axis (K2) and a short axis (K3). Each of these tensors is comprised of a relative intensity (i.e., a multiplier of the bulk susceptibility) for that tensor (e.g., column CJ) a declination (or dip Azimuth: e.g., column CM) and vector inclination (or plunge: e.g., CP) and alpha 95 errors for each (e.g., CS and CV). The AMS ellipsoid is geographically corrected relative to drill-hole or surface sample orientation and can be visualised using stereonets.

Anisoft 4.2 was used to assess the quality and clustering, whether the magnetic fabrics within specific lithologies or structures have a preferred orientation overall and whether the distribution of orientations reflect a specific type of fabric within that rock

https://doi.org/10.5194/essd-2023-464
Preprint. Discussion started: 20 February 2024

(e.g., axial, axial planar or planar distributions: Závada, et al., 2017). Three main parameters, introduced by Jelinek (1981), are commonly calculated from the results to differentiate the style of fabrics present. P (e.g., column DA) is equal to K1/K3 and corresponds to the anisotropy factor. Rocks with high P values are highly anisotropic, whereas rocks with P≈1 are isotropic. L (e.g., column CY) is equal to K1/K3 and defines the extent to which a rock has a lineation (i.e., if K1>K2≈K3 the ellipsoid is prolate and the rock has lineation). F (e.g., column CZ) is equal to K2/K3 and defines the extent to which a rock is foliated (i.e., if K1≈K2>K3 the ellipsoid is oblate, and the rock has a foliation). Other Jelinek (1981) parameters included, are Pj (e.g., column DB) the corrected degree of anisotropy which takes the shape parameter into consideration and T (e.g., column DC) the shape parameter (0=isotropic; +1>T>0 = oblate (planar) ellipsoid; -1<T<0 = prolate (linear) ellipsoid). An example data output from Anisoft 4.2 software and an interpretation of that data are presented in Figure 18.

Processing

The data collection process involved individual analysis of up to three specimens (i.e., sub samples) for some properties (e.g., magnetic susceptibility), up to three samples simultaneously for others (e.g., radiometrics), and only one specimen but one was analysed for other (e.g., TIMA). It is not practical to present this data as a database, due mainly to the extent of additional calculations and metadata required by each of the individual techniques included. Instead, a simple excel spreadsheets (refered to as a database) is used.

In the Cloncurry METAL database (Austin et al., 2021d), because there are multiple measurements per sample, and because the AMS ellipsoids are vector quantities, further processing is required to produce bulk structural fabrics for samples. Trigonometric vector addition was applied to calculate weighted mean lineations (i.e., K1 vectors: columns FK-FL) with corresponding intensity (column FM) and weighted mean foliations (i.e., inverse weighted planes to K3: columns FO-FP) with corresponding intensity (column FQ) for each sample. These calculations, which incorporate both vectors and the relative intensity of the fabrics provide weighted mean foliation and lineation data for each sample, which are compatible with traditional measurements used in structural geology.

Mean length is also calculated for the mean lineation (column FN) and mean foliation (column FR) as a measure of certainty of the results. The mean length is the vector sum of two or more vectors divided by the sum of the vector lengths (i.e., a measure of the parallelism of the vectors) which provides an effective measure of the relative textural homogeneity of the sample. Samples with a mean length >90% are considered texturally consistent. Whilst sample with mean length <90% have fabrics that are inconsistent to at least some degree the user should note that the result is highly dependent on the number of vectors used in the calculation. Regardless of the number of vectors included in the calculation, a mean length of 100% indicates all vectors are parallel. Where two vectors are used in the calculation, a mean length of 95% approximates two vectors of equal intensity are 30˚ offset from each other; a mean length of 85% approximates two vectors of equal length offset 45˚ from each other; and a mean length of 50% approximates two vectors of equal length offset 90˚ from each other. Where three vectors are used in the calculation a mean length of 92% approximates three vectors of equal intensity are 30˚ offset from each other; a mean length of 80% approximates three vectors of equal intensity are 45˚ offset from each other; a mean length of

https://doi.org/10.5194/essd-2023-464
Preprint. Discussion started: 20 February 2024

33% approximates three vectors of equal intensity are 90˚ offset from each other. Where three vectors are used in the calculation a mean length of zero is possible (but highly unlikely) if three vectors of equal intensity are offset 120˚ from each other.

3.2.7 Automated Mineral Mapping

Sample Preparation

After the petrophysical analyses were completed, samples were polished for automated mineral mapping. Where possible, the rounds were polished on the side opposite to the Palaeoazimuth markings (see Section 3.1) and without resin impregnation on the surface, however resin was required for more porous samples.

Automated mineral mapping was conducted using a Mira Tescan™ field emission gun (FEG) scanning electron microscope (SEM), coupled with three EDAX Energy Dispersive X-ray Spectroscopy (EDS) detectors, a backscatter electron (BSE) detector and the Tescan Integrated Mineral Analyser (TIMA) software package. The automated modal mineralogy setting on the SEM utilises a 25 keV, 6 nA, 26 nm electron beam and a 10 µm pixel size was chosen for analyses with a required minimum of 1000 X-ray counts per pixel. Standard electron beam alignment, focussing and instrument calibration, including BSE and EDS detector calibration, were carried out before each analysis run of up to 22 samples.

An area ~23 mm in diameter of the polished surface was scanned, with an average analysis time of 1 hour and 50 minutes at 10 µm pixel resolution, producing mineral phase and BSE data for each sample. If the SEM scans over an unrecognised mineral phase, a grain boundary, or poorly polished section due to the presence of clay minerals or sample fractures, unclassified (black) pixels will occur in the dataset and in the phase panoramas. Any unrecognised, genuine phases can be later added mineral library in the TIMA software. While the TIMA SEM system is operating in modal mineralogy mode, it produces volume percent mineral abundances down to 0.01 vol. % detection limits, which can be exported as a .csv along with the mineral phase.png images (e.g., Figure 19) that are integral to interpreting alteration mineral assemblages and textural relationships of each sample.

Mineral Classification Methods

For each of the deposits studied in this project, a CSIRO-developed, X-ray spectra-matching mineral classification library was generated. The ‘legacy’ Uncover Cloncurry samples were considered in the development of each library and were reprocessed accordingly. The new mineral classification libraries have improved previously misclassified or unclassified phases (i.e., scapolite and plagioclase at Ernest Henry and sillimanite/andalusite and pyroxenes at SWAN) found in the Uncover Cloncurry datasets. On average, each of the deposit-specific mineral classification libraries include more than 150 minerals, which have been generated from international standards from Web Mineral’s Mineralogy Database, semi-quantitative Electron Backscatter Diffraction (EBSD) analyses, which were acquired with an Oxford detector on the TIMA SEM, or microprobe standards. Any minerals that were imported directly from the international Web Mineral database were done so in consultation with the

https://doi.org/10.5194/essd-2023-464
Preprint. Discussion started: 20 February 2024

available literature for each of the deposits and in-built spectra-matching and spectra-quantification calculators in the TIMA software.

In the mineral classification library, each mineral is constrained by its mineral chemistry (Figure 20) and furthermore, the expected X-ray count range per element within the mineral. The X-ray count ranges are guided by the reference spectra, but generally need to be refined for each mineral as the computed ranges can be misleading. Additional elemental constraints with low-to-background X-ray count values are often added when minerals of similar composition need to be differentiated (Figure 21). Due to many minerals existing as variations of their solid solutions, in some cases, small impurities such as Fe and Mg in muscovite (Figure 21) are allowed into the mineral definition. The primary and secondary constraints are particularly important for minerals that have undergone multiple stages of alteration and include common and unusual impurities, for example the grossular- and spessartine-rich almandine garnet species found at the Cannington deposit (Pearce et al., 2021).

3.2.9 Geochemistry

Portable XRF data were collected using an Olympus Vanta pXRF instrument, which has a 50 kV, 4-Watt rhodium (Rh) X-ray tube and a large-area Silicon Drift Detector in GeoChem mode (10 kV and 40 kV beam). The measurements were checked against 5 known diamond core standards which were matrix-matched, however the data presented in the database is uncalibrated against the standards as the instrument measurements closely matched the standard values. The instrument drift was also monitored by repeating one unique standard and a blank every 20 analyses. Measurements were taken on the polished surface of the TIMA rounds apart from samples which were set using resin prior to polishing due to poor rock quality/friability (e.g., some SWAN samples). The resin has a significant impact on the pXRF results due signal attenuation and interference, and so measurements were undertaken on the unresined back of the samples. The front resined sides were also measured for small test set of 23 samples from SWAN, confirming that the data are unusable as all elemental concentrations are attenuated by as much as two orders of magnitude. All pXRF data in the database (columns NY to QQ) includes the proportion of the element present and associated reading error (1 standard error), both of which are displayed in parts per million (ppm). Light elements, defined as those with atomic number <11 (i.e., Na and lighter) cannot be quantified by pXRF and so the total proportion of all light elements (LE_concentration) is presented however in columns QP, with the respective error in column QQ (both in ppm).

3.2.10 Hyperspectral Data

Data Collection

Hyperspectral data in the VNIR-SWIR (350-2500 nm) spectral regions was collected using ASD (Analytical Spectral Device) Fieldspec4 spectrometer. Data was collected on the polished TIMA round surfaces for 100 averages, and the instrument was calibrated with using a standard white reference material. Spectra were viewed and analysed in The Spectral Geologist (TSG) software. Collecting spectral data on a polished surface is not the ideal measurement condition and imparts some noise on the

https://doi.org/10.5194/essd-2023-464
Preprint. Discussion started: 20 February 2024

spectra due to scattering effects which are largely related to the mineral assemblage present (e.g., more sulphide or iron oxide rich samples are generally noisier). However, hyperspectral measurements were not a component of the original Uncover datasets and were added as a database component for the METAL datasets mid-way through sampling, and so a significant number of METAL samples as well as the ~500 Uncover Cloncurry samples were already polished prior to the onset of data collection.

A key component of creating a fully scalable and integrable geoscience database, is that all the data are measured in a consistent manner with measurements from different methods on the same sample surface. And so, a suite of 23 test samples from Ernest Henry were measured pre and post polishing, to evaluate the impact of polished vs. unpolished samples on the spectral results. The primary difference between the spectra from the rough and polished surface is in the overall shape of the spectral background which is observed as systematically lower VSalbedo (reflectance albedo over 450-2450 nm) and higher SWIR spectral contrast pfit (range of reflectance over [1300,2500] nm, de-trended by a 3rd order poly fit) in the polished samples (Figure 22). A minor but systematic difference is also observed in the spectral outputs from polished and unpolished samples for commonly used scalars (e.g., 2250D and 2200D). However, the outcome is the same trend across the sample suite for both the polished and unpolished sample, and negligible changes to the qualitative TSA (uTSAS) outputs were observed (Figure 22). Given the test sample results and that the bulk of the samples (including all of the Uncover samples) were already polished, the remaining samples were also measured on the polished surface for consistency across the database so that all measurements (TIMA, pXRF, ASD) were representative of the same surface. The exception is for samples which were set using resin prior to polishing due to poor rock quality/friability (e.g., some SWAN samples). As with the pXRF data, the backside of the resined samples was measured to avoid interferences from the resin.

Processing and Data Outputs

Spectral mineralogy outputs were generated in the TSG (The Spectral Geologist) software using a series of CSIRO-developed Batch Scalars (system, user published, and file) as well as the inbuilt TSA (The Spectral Assistant) function of TSG. These standard outputs were included for each deposit dataset regardless of their efficacy for a given deposit or mineral system. This so that every deposit has consistent outputs for use in advanced data analytics and relies on the user for evaluation of which outputs to use in making interpretations. All the spectral outputs have been created using TSG Version 8.0.7.4 and TSA Version 7 (released May 2020).

TSA is an algorithm for automated spectral unmixing which uses its training library to match the spectrum against a single mineral or model a simulated mixture of 2-4 minerals that most closely resembles that of the input spectrum (Berman et al., 2011) (Figure 23). TSA mineralogy outputs are one of the most common outputs derived from hyperspectral data using TSG and should be used with caution as they are only a best approximation of the top three contributing minerals to a given SWIR, VNIR, or TIR spectrum, and represent relative abundances. The quantification of any spectral parameters requires the concurrent collection of validation data for calibration of the spectral data, e.g., quantitative XRD (Haest et al., 2012; Laukamp et al., 2017) or EPMA (Lypaczewski and Rivard, 2018). Regardless, TSA unmixing results are commonly used by geologists

https://doi.org/10.5194/essd-2023-464
Preprint. Discussion started: 20 February 2024

as the data are exported as relative weights of a given mineral (Figure 23), however, these results and their reliability are highly dependent on the reference library used, as well as the mineral assemblage present (Laukamp et al., 2017). It should also be noted that the mineral assemblages present in the Cloncurry METAL and Uncover samples are dominated by SWIR-inactive minerals, including oxides and sulphides, where the SWIR-active mineral assemblages relevant for vectoring towards mineralisation are typically dominated by chlorite, biotite, and calcite mineral species (e.g., Ernest Henry) which are challenging to distinguish between in the SWIR due to their overlapping spectral absorption features in the SWIR, namely the ~2250 nm "Mg-OH" and the ~2340 nm carbonate feature (Laukamp et al., 2017; Lypaczewski and Rivard, 2018) (Figure 23). TSA results have been exported into the Cloncurry METAL database (Austin et al., 2021d) at both at the Mineral Group (QW to RJ) and Mineral scale (RK to TE) to allow for application at different scales of detail. However, the Mineral Group results are more robust, and the mineral scale of TSA outputs should be approached with caution (e.g., Laukamp et al., 2017). Parameters related to the quality of the fit have also been included to assist the user in evaluating the quality of the results (QS to QV) (Figure 23). The minerals included in the TSA library for a given deposit are informed by the TIMA automated mineralogy results with domain expert input to evaluate the rate of false positives and misclassifications. Given the limited number of SWIR active minerals in the samples, the libraries used for the TSA unmixing do not change significantly between deposits. For all samples, the Albedo threshold in the TSA setting was changed from its standard setting of 0.04 to 0.01 to accommodate the darkness of the rocks, and the lower albedo of the polished samples with respect to unpolished or powdered samples. This also reduced the number of NULL TSA results.

As discussed above, for the purpose of the database outputs and their application in advanced data analytics, the TSA libraries have been minimally changed between deposits, and the TSA settings have been kept consistent. However, the TSA outputs for a given deposit may be improved (NULL results reduced) for certain mineral phases with the addition of deposit specific custom external reference libraries and further tweaking of the TSA settings. The changing of TSA settings is something which is generally not recommended and was tested for Ernest Henry with well constrained TIMA mineralogy and domain knowledge input. While the number of null results were reduced, the results were often unreliable as would be expected when removing constraints from unmixing model, and in general resulted in an overrepresentation of chlorite across the dataset (e.g., EHM025 in Figure 23), and so the results are not included in the database. Another approach to improving unmixing results is to expand the mineral library using external reference libraries which include spectra of minerals known to be in the dataset. This approach was tested with the Ernest Henry dataset using a custom external library which included a larger number of biotite spectra, as biotite and chlorite are difficult to unmix, as well as scapolite which is known to occur in the samples (from the TIMA data). The application of this library did not result in a significant improvement in the unmixing results (e.g., no scapolite identification) and in many cases resulted in more misclassifications, and so the results are not included in the database. The presence of known phases (from previous GSQ work and CSIRO TIMA datasets) such as scapolite and piemontite were also probed using a spectral matching method (aux-match in TSG). This method outputs the results of curve matching between spectra in the project dataset and spectra in an Aux (Custom Library) dataset and yielded no significant matches despite the presence of scapolite in abundances of up to ~50 wt% in some samples.

https://doi.org/10.5194/essd-2023-464
Preprint. Discussion started: 20 February 2024

This highlights the inherent difficulties mineral identification in mixed samples from SWIR spectra using endmember library spectra. Another limitation of conventional unmixing methods (like TSA) is that it uses only the SWIR region of the spectra (1400-2500 nm) and does not consider the entire spectral range of the instrument (350 – 2500 nm) (Figure 23). This is important when considering that the assemblages present in the Cloncurry samples are dominated by "SWIR-inactive" minerals and that the mineralised assemblages are iron-oxide rich (Figure 23). While SWIR inactive mineral such as feldspars do not have distinctive spectral features in the SWIR they contribute to the spectral background, and the VNIR region of the spectrum is sensitive to the presence of iron oxides and transition metals. It is for this reason; that the entire raw spectrum is included in the database.

Given the inherent complications with spectral unmixing results, many spectral geologists (e.g., Laukamp et al., 2021) prefer to probe individual spectral features in a dataset by looking at for example, the depth, wavelength or shape of a well understood spectral absorption feature such as the 2200 nm "Al-OH" feature (e.g., Haest et al., 2012) or the 2250 nm "Mg-OH" feature (e.g, Sonntag et al., 2012) (Figure 23). Figure 23 provides a good example of how the 2250D (batch system) scalar, which provides a measure of the depth of the 2250 nm feature, relates to abundance of chlorite in three samples and is an improvement on the TSA outputs. Scalar is the term used by TSG to refer to any set of calculated values related to loaded spectral data. The outputs included in the database are what are referred to as batch scalars. These are pre-written, well-established, and in most cases published scripts for spectral parameters which probe the position or depth of a given spectral absorption feature (See Laukamp et al., 2021 for an overview). The outputs in the database are split into three categories, TSG Batch System Scalars (scalar name_SS), TSG Batch User Scalars (scalar name_US), and Batch File Scalar (scalar name_FS). Batch system scalars commonly use a 3-band polynomial fit, while the User Scalars employ a Multiple Feature Extraction Methods for their outputs so are much more restrictive (Figure 24). Details of the scalars name, application, as well as references are included the database explanatory notes and are also described in Laukamp et al. (2021). Not all of the scalars in the database will relevant or even trustworthy for every deposit but have been included so that each dataset in the final database (Austin et al., 2021d) has the same outputs for use in advanced data analytics. It is also important to note that the System Scalars (_SS) do not have any masking applied to them, and that the user should consider this in their application (Figure 24).

3.3 Dataset collation and integration

For ease of use, our dataset is provided as a single excel spreadsheet or as separate spreadsheets for individual deposits. It comprises numerous outputs from a variety of different sensors, which are processed in numerous software platforms, and required additional pre-processing, integration, and assimilation steps for some of the methods.

The format was modified from the previous version (Uncover Cloncurry: Patterson et al, 2016), which had three to four lines per sample each corresponding to a different sub-sample (specimen). This format was difficult to use because most data was missing from most lines. In the updated version, all data from each sample (up to three specimen) are included in one row, and extra calculations have been added to better summarise the data. In general, these are simple averages. However, in the case of vector quantities (e.g., AMS and remanent magnetisation) the average direction of three vectors coupled with the average

https://doi.org/10.5194/essd-2023-464
Preprint. Discussion started: 20 February 2024

intensity of the vector can provide a poor summary of the data and the associated errors. Calculating vector means (i.e., adding the three vectors together trigonometrically) is a far more accurate summary of the data and the associated mean length metric provides an excellent measure of the consistency of the three vectors used in the calculation.

To make the Cloncurry METAL data (Austin et al., 2021d) easy to use a range of metadata (descriptions of which are outlined on Tab 2 of the database) are provided, including:

1. Information on the structural context and system zonation have been included. Structural context is ascertained by examination of the position of the samples relative to mineralisation (determined from Leapfrog interpolation) and relative to the established structural framework of deposits (if they exist). Where possible previous work, including 3-D geophysical and geochemical models and cross-section in a 3-D GIS (e.g., Discover 3D™, Geoscience Analyst™, or Leapfrog™) was assembled. System zonation was determined by examination of the alteration assemblages present in TIMA imagery and is also determined relative to previous work. An example of how this contextual metadata is used is provided in relation to structure, geophysics and geochemistry in some of the major outputs of this study (e.g., Schlegel at al., 2021; Austin et al., 2021 b, c; McFarlane et al., 2021, Stromberg et al., 2021).
2. Accurate three-dimensional location data (X, Y in metres relative to GDA zone 54 map grid) and collar altitude (Z relative to sea level) for each sample is also provided. XYZ data were calculated from collar location and survey information from confidential company drilling data and downhole depth information collected during sampling and computed using the "Drillholes" function of MapInfo Discover™.
3. General geological descriptions based on company logs (where available), from sampling notes (where available) and/or from TIMA imagery are also included. It should be noted that these data are highly qualitative, especially the former two. Whilst the TIMA images are quantitative, consistent representations of the lithology of the rock, the interpretations of the rock type, alteration and texture are still qualitative. Until complex variables such as protolith, textural fabrics and relative proportions of alteration products can be determined autonomously from TIMA imagery using data analytics, these descriptions will have to suffice. However, they should be used with caution, and users of the database are encouraged to review the TIMA imagery themselves and revise the structural and alteration framework to suit their specific needs, or better still, devise an automated method.

3.4 QA/QC

Each of the input datasets for this project were produced using proprietary instrumentation and software, and as such much of the quality assurance and checking was undertaken using these software packages prior to export. Some of the main problems identified at this stage of the process included:

1. False parallelism of NRM directions due to the sample rotator not working correctly on the JR-6 magnetometer.
2. Subdued magnetic susceptibility readings in magnetite-rich samples due to self-demagnetisation effects.
3. Large percentages of "unknown" minerals in TIMA due to TIMA mineral library limitations.

https://doi.org/10.5194/essd-2023-464
Preprint. Discussion started: 20 February 2024

These issues and others of a similar nature were easily addressed by minor changes to the set-up of various instruments, modifying instrument settings and/or improving reference spectra, as required.

The processing and assimilation of these individual data streams, however, present far more opportunities to introduce errors via mistranslation of proprietary data formats into text, misplacement of data, or misapplication of functions (e.g., using the wrong columns to calculate averages and ratios). By and large these kinds of errors presented as obvious bipolar contrasts in resultant outputs, typically with orders of magnitude variance. These were (hopefully) all fixed prior to publication.

In some cases, the data passed QA/QC but still had a major flaw that made it difficult to integrate effectively. These were encountered in a subsequent data analytics project (Williams et al., 2022) in which the entire dataset produced a suspicious bi-modal clustering on one axis of several non-linear data reduction projections. After individually assessing each of the various components which correlate with a key axis of the dimension reduction projection, two major problems were identified. Both were related to underlying collection and processing issues out of our control.

1. An approximately 10% difference in the radiometric dose, mainly correlated with a consistent difference of ~25% between the Potassium% of two groups of samples. Those with lower dose rate were all measured at our North Ryde laboratory around November 2018, whereas the samples with the higher dose rate were all measured at our relocated Lindfield laboratory around April 2020. Williams et al., (2022) found that all samples measured at each site shared the same flaw and inferred that the contrast in mean radiation level was due to the background radiation of the different laboratory environments. This has been amended by normalising each channel of radiometric data relative to the mean measurements from each site.
2. Williams et al., 2022 also found instances where in which similar rocks with similar mineralogy plotted at opposite ends of a dimensionally reduced projection. In this case it was found that the main difference between the two clusters was related to how the TIMA mineralogy maps were generated. One of these clusters was comprised of earlier Uncover Cloncurry Samples (Patterson et al., 2016) which were measured using a previous version of the TIMA software and processed with a slightly different TIMA library. The previous TIMA library did not include phases such as fayalite, almandine, epidote, fluorite, scapolite, and others. Thus, during processing of the data, one mineral could easily be incorrectly classified as another, e.g., andesine in the earlier data was instead classified as scapolite in the later. In some instances, the same mineral was also mapped using different names, e.g., potassic feldspar was mapped as microcline in the Uncover Cloncurry mineral library, but as K-feldspar in the Cloncurry METAL library (Williams et al., 2021). In general, the use of a different TIMA library may dramatically affect several mineral phases and in this case variances in the volume of actinolite, scapolite and k-feldspar, all affected the projection dramatically. Because of the updated software it was not feasible to individually reprocess all results and so legacy samples were only reprocessed for deposits studied in the Cloncurry METAL project (i.e., Cannington, Ernest Henry, SWAN, Starra-276, Osborne, and Eloise).

This meant data from the earlier study could not be easily integrated with data from the latter, highlighting that the processes by which data are collected, reduced and represented have profound impacts on any big data approaches to geoscience. This is particularly the case for categorical data (e.g., mineralogy) which may not be precisely identified or may correspond to

https://doi.org/10.5194/essd-2023-464
Preprint. Discussion started: 20 February 2024

mixtures of multiple endmembers. But it is a common problem across all spectral/elemental imaging and scanning analyses where data needs to be 'unmixed'. To best address such issues across different rock suites using quantitative mineralogy approaches (e.g., SEM-TIMA) it is critical to 1. have access to raw data, 2. customised data reduction approaches, and 3. Smarter and/or more flexible approaches to classification/estimation of mineral phase proportions.

Data collection issues almost certainly have a greater impact on outputs than data analytics methodologies. The issues identified here are detectable, resolvable, and have relatively small impacts due to the scale integrated nature of the data, the high quality of the data and consistency of the sampling and analytical tools used. However, the use of datasets assimilated from different scales, resolutions, precisions, and tools, more generally would almost certainly lead to far more serious issues, which could be substantially less detectable, and which no amount of buffering, filtering, recalibration, or conversion can adequately supress. The consistency and quality of inputs is paramount.

5. Applications

The data collected by this study span a range of geoscience applications, including understanding deposit paragenesis (Schlegel, 2021, Schlegel et al. 2021, 2022), integrated insights into the geochemical, mineralogical, and petrophysical footprints of mineral deposits (e.g., Austin et al., 2021 b), quantifying the structural controls (Austin et al., 2021 c; McFarlane and Austin, 2021) and geophysical expression (Austin, 2021 a, b) of mineral systems. The resulting knowledge can be applied to three broad functions, Mineral Exploration Techniques, Minerals System science and characterisation, and novel approaches to each using data analytics.

5.1 Mineral Exploration and Minerals System Characterisation

The data produced has applications across a range of green and brownfields exploration toolkits as visualised by the Venn diagram in Figure 25. At the core of this capability is the SEM-TIMA quantitative mineralogy technology. SEM-TIMA provides quantitative information about mineralogy, lithology, rock texture, metamorphic grade and alteration paragenesis, much of which is only collected qualitatively and very subjectively in mineral exploration. Furthermore, SEM-TIMA provides contextual information that can be used to constrain our understanding of the other techniques (i.e., surrounding TIMA in the Venn Diagram (Figure 25)) producing camp-scale exploration targeting criteria which can be exploited using conventional core-shed tools (e.g., Figure 26). The resultant data also provide quantitative constraints across a range of geoscience disciplines, which address the five questions of mineral systems science (Walshe et al., 2005), including: (1) What is the role of Geodynamics? (2) What is the role of Architecture of the system? (3) What are the roles of fluids, their sources and reservoirs? (4) What are the fluid flow drivers and pathways? (5) What are the metal transport and deposition processes? The applications of these data are discussed citing examples within this framework below.

https://doi.org/10.5194/essd-2023-464
Preprint. Discussion started: 20 February 2024

5.1.1 Geodynamics

Insights into the geodynamics of the minerals system can be gained via interrogation of the mineralogical and textural information derived from the SEM-TIMA imagery. The mineralogy data provides information about the relative abundance of metamorphic indicator minerals (e.g., sillimanite, andalusite, kyanite pseudomorphs) as well as information about the temporal juxtaposition of metamorphic and metasomatic reaction assemblages. Textural information from SEM-TIMA also provides insights into tectono-metamorphic evolution by differentiating primary sedimentary and igneous textures from metamorphic, metasomatic, and tectonic textures. This mineralogical and textural quantification of rocks provides valuable information for the reconstruction of sedimentary, magmatic, metamorphic, tectonic, and metasomatic history, i.e., the geodynamic evolution, of a terrane. In general, for the Cloncurry terrane, mineralisation typically post-dates the major metamorphic and tectonic episodes, coinciding instead with late magmatic hydrothermal activity and strike-slip tectonics. However, there are examples in which our data provide critical insights into the earlier metamorphic history of the Cloncurry district. For example, the work by Pearce et al. (2021) integrating metamorphic petrology and REE-geochemistry data from the Cannington deposit identifies a complex history pervasive Fe- and Ca-Fe alteration, that was subsequently exposed to high-grade (>upper amphibolite facies) metamorphism and later hydrated to form the complex assemblages observed. The TIMA imagery on their own provide future studies with an ideal launching platform, allowing researchers to readily locate minerals of interest for interpreting broad crustal processes (e.g., REE profiles), thermobarometry (e.g., garnet, pyroxenes, amphiboles, sillimanite) and geochronology (e.g., monazite, zircon).

5.2.2 Architecture

The mineralogical and textural quantification of rocks provided by SEM-TIMA can be integrated with quantitative information on rock fabrics provided by anisotropy of magnetic susceptibility (AMS) data to provide valuable information about the architecture of the system. The AMS technique allows us to differentiate isotropic vs anisotropic rocks, thereby assisting differentiation of rock types and providing insights into their role in the development of regional to deposit scale architecture. For example, Austin and McFarlane (2021) found that dioritic intrusions in the distal foot and hanging wall of Ernest Henry had isotropic (i.e., undeformed) fabrics, consistent with them acting as rigid buttresses that focussed strain during deformation. AMS provided information on the nature of fabrics within different rock types, and in particular whether fabrics are lineation or foliation dominant and the strength of those fabrics. Such information allows us to differentiate primary sedimentary and magmatic fabrics from tectonic fabrics and furthermore quantify the bulk rotations in those fabrics related to folding (e.g., McFarlane et al., 2021) and/or rotation of rigid blocks within an incompetent substrate (e.g., Austin and Patterson, 2020). The technique furthermore allows us to contrast lineation and foliation fabrics within a cluster of samples to produce information of the kinematics of a deposit. Such insights can be integrated with convention structural geology, lineament interpretation based on geophysical filter products and 3-D geophysical models to characterise regional architecture and paleo-kinematics.

https://doi.org/10.5194/essd-2023-464
Preprint. Discussion started: 20 February 2024

5.2.3 Fluids (metasomatism)

Fluid composition (including contained elements such as gold, copper, iron, sulphur and carbonate carbon) and fluid properties (including oxygen fugacity/redox) and acidity (pH)) are important factors that control mineralisation. Whilst technically not directly characterised by the data obtained in this study, valuable insights into fluid composition, redox and acidity of the fluids involved in mineralisation can still be obtained via understanding of alteration paragenesis and deposit zonation. The main tools for understanding these properties include SEM-TIMA mineralogy and SWIR hyperspectral data.

The Cloncurry METAL datasets identified several mineral zoning patterns and compositional trends related to the Cloncurry District IOCG systems, many of which are non-unique, and have applications to district scale exploration. These include:

1. Feldspar mineral zonation at Ernest Henry (e.g., Schlegel et al., 2021) and Eloise (e.g., Birchall et al., 2021)
2. Zonation in white mica and carbonate abundance and chemistry at Starra-276 (McFarlane et al., 2021a)
3. Chlorite and biotite distribution and/or chemistry at Eloise (Birchall et al., 2021), and Osborne (McFarlane et al., 2021b)
4. Chlorite-biotite-white mica zonation at Ernest Henry (Schlegel et al., 2021) and Mt Elliot (Stromberg et al., 2021a)
5. Apatite haloes around the mineralised zones at SWAN (Stromberg et al., 2021a), Ernest Henry (Schlegel et al., 2021) and Eloise (Birchall et al., 2021)

Hyperspectral data are sensitive to most mineral species (apart from sulphides), and different spectral ranges are sensitive to different mineral species (Laukamp et al., 2021). While hyperspectral mineralogy is a surface technique, it can be used to map alteration from the sub-sample to regional scales, and thus can be easily integrated with other geoscience datasets such as radiometrics and magnetics to inform our understanding of alteration footprints and fluid pathways (e.g., section 5.2.4). Stromberg et al (2021) provides an excellent example, combining high-resolution SEM-based mineral mapping from four drill holes at SWAN-Mt Elliot with continuous downhole hyperspectral HyLogger3™ datasets to present an updated alteration paragenesis of the system. Their work describes the role of successive fluids in localising mineralisation and developing the associated alteration footprint.

The role of fluids in localising mineralisation can also be examined at much finer scales using the SEM-TIMA coupled with geochemistry data. Schlegel et al. (2021) and McFarlane et al. (2021) highlighted the role of acid-base reactions in controlling mineralisation at Ernest Henry and Starra-276. Schlegel (2021, 2022) furthermore highlighted how SEM-TIMA mineral mapping approach can be used to understand the role of fluids in generating porosity in hydrothermal systems. They suggested that mineral zonation resulting from of sodic alteration, potassic, and iron metasomatism, shearing, and brecciation, followed by regressive hydrolytic alteration and carbonatization. Hydrolytic alteration, resulted in variable replacement of magnetite by hematite, also resulted in volume reduction/porosity creation (evident now as late carbonate infill and veining) which made way for the late, high grade copper mineralisation.

https://doi.org/10.5194/essd-2023-464
Preprint. Discussion started: 20 February 2024

5.2.4 Pathways

Insights from convention structural geology, geophysics-based lineament interpretation and 3-D geophysical modelling provide rigid constraints on the architecture of the system to and its paleo-kinematics. Structures are commonly assumed to be fluid pathways. In reality, however, all structures have unique histories, have different kinematics, and are active at different times. Whilst the interaction of structure and alteration can be constrained at the sample to deposit scale using METAL data, it is more difficult to differentiate the role of regional structures in localising mineralising fluids based purely on convention structural geology and lineament interpretation. To differentiate fluid pathways from other structures new methods are required that can highlight fluid rock interactions within those structures, not only at the sample scale to core scale, but also at the district scale.

Research on IOCG deposits (Austin et al., 2016 b, i; Austin and McFarlane, 2021; Austin, 2021 b; Austin et al, 2021 c) has identified associations between mineral deposition and redox reactions, reflected in transitions between magnetite and pyrrhotite, or hematite bearing lithologies. That work illustrated that transitions between these key deposit forming minerals coincide with elevated uranium on the more oxidised side of the gradient (i.e., magnetite in a reduced system, or hematite in an oxidised system). This association is mappable at the sample scale using METAL approach, at the drill core/ deposit scale using a handheld susceptibility meter and gamma-ray spectrometer. At a regional scale the association of Fe-oxide and uranium (i.e., the redox gradient) can be mapped using a combination airborne magnetic and radiometric data (e.g., Austin, 2021 b). This technique allows the differentiation of fluid pathways from un-involved structures at several IOCG deposits across the Cloncurry district including SWAN, Starra-276, Monakoff, Cormorant and Canteen (Austin, 2021b, Austin et al., 2021d). The recognition of such processes provide and ideal proxy for oxidised fluid pathways within IOCG mineral systems because they allow use to convert chemical reactions into physical properties that can be recognised in geophysical data. In contrast to mineralogical or chemical properties, these physical properties be readily scaled from sample to drill-core, to deposit to district, allowing us to trace fluid pathways from the deposit into the district.

5.2.5 Mineral Deposition

Mineral deposition in hydrothermal systems it typically a function of several processes, usually the chemical reactivity potential of the host and fluid, coupled with the available porosity (e.g., section 5.2.3) and structural controls. The Cloncurry METAL database (Austin et al., 2021d) provides insights into each. Information on structural fabrics within a mineralised system is derived primarily from AMS data (discussed in 5.2.2), which is upscaled using geophysical modelling and lineament interpretation and integrated with insights from radiometrics to constrain fluid pathways (discussed in 5.2.4). This knowledge of the structural controls is coupled with insights into different fluid-rock reactions and alteration paragenesis from SEM-TIMA (discussed in 5.2.3) to characterise mineral deposition. In essence, the processes involved in mineral deposition are interdependent, that is fluid pressure impacts structural rheology, which impact porosity generation, which impacts chemical

https://doi.org/10.5194/essd-2023-464
Preprint. Discussion started: 20 February 2024

reactivity. These processes are all linked, and the great advantage of the METAL methodology for data integration is that our data are integrated-by-design and therefore describes these processes holistically.

Austin and McFarlane (2021) provide an example of how insights into structural controls can be integrated with an understanding of the metallogenic history to understand mineral deposition. Their work demonstrated that the juxtaposition of tectonic lineations and foliations at Ernest Henry suggested anticlockwise rotation of the strain direction causing a transition from pure reverse movement to sinistral strike slip from ca 1550-1500 Ma. They interpreted that as the system evolved into strike-slip dominant tectonism, in which N-S oriented near surface structures linked with reactivated sub-parallel basement structures facilitating fluid flow between the lower and upper crust. The AMS technique has furthermore identified that the majority of structurally controlled hydrothermal deposits plunge parallel to the measured K1 (lineation) vector (e.g., Austin et al, 2016 d,e,f; Austin and McFarlane, 2021, McFarlane et al, 2021, Birchall et al, 2021). This allows us to predict the plunge of most mineral deposits in the Cloncurry District, demonstrating its value as an exploration tool, if utilised early in a greenfields drilling campaign to accurately plan follow up drilling (McFarlane and Austin, 2021).

5.3 Machine Learning

Williams et al. (2022) developed targeted workflows to make use of the range of geoscience data within the reference database and investigated options for pre-processing, transformation, and the construction of unsupervised and supervised predictive models. These workflows were implemented in Python and were presented as a package of configurable scripts, which can be readily integrated and extended with widely used open-source machine learning packages. A range of software tools and algorithms have been used, adapted and created to make use of specific types of geoscience data in machine learning workflows and for configuration of model generation and interrogation.

The multi-property nature and dimensionality of the dataset presented a challenge for use in machine learning workflows, targeted dimensionally reduced projections were found to be useful for unravelling complex geology than bivariate, ternary or three-dimensional diagrams. Williams et al (2022) identified the prominent features and signatures which define the larger scale structure of these projections providing a geological framework for the clustering models developed. Dissection of dimensionally reduced projections also assisted in identifying a series of QA/QC issues related to the reference dataset itself, which otherwise may have been more difficult to identify or diagnose.

The models developed can efficiently represent complex geology as described by geologists and suggest that some degree of predictive analytics for exploration is feasible. The project provided a reference framework (Figure 27), allowing explorers to contextualise future exploration results relative to known mineral system signatures in the region, and in so doing further building the reference framework.

Data Availability

Data described in this manuscript can be accessed from The Geological Survey of Queensland (GSQ) Open Data Portal: https://geoscience.data.qld.gov.au/data/dataset/cr126168/resource/geo-doc1310615-cr126168 (Austin et al., 2021d)

https://doi.org/10.5194/essd-2023-464
Preprint. Discussion started: 20 February 2024

Conclusions

Cloncurry METAL set out to push the boundaries of "Big Data", by critically examining the role of the data, in particular the pitfalls of incompleteness, inhomogeneities of scale and specific scale dependencies of different data types (e.g., contrasting depth of resolution of magnetic vs gravity inversions). We recognised that one way to bridge the gap between large-scale, low-resolution datasets and the fractal (i.e., multi-scale) nature of geological systems, was to develop a scale consistent (sample-based) methodology for data collection, and translate the knowledge into physical parameters, which are readily scalable. The outcome of which is led to the world's first, fully integrated, petrophysical-mineralogical-geochemical-structural-metasomatic characterisation dataset, across over twenty deposits from the most geologically complex mineral systems on Earth.

This study presents data, from this innovative district-wide, scale-integrated, geoscience data project, which analysed 1,590 samples from 23 mineral deposits and prospects across the Cloncurry District, Queensland. Ten different analytical techniques, including density, magnetic susceptibility, remanent magnetisation, anisotropy of magnetic susceptibility, radiometrics, conductivity, modal mineralogy from SEM-TIMA, geochemistry, and short-wave infrared (SWIR) hyperspectral data resulted in 561 columns of scale-integrated data (+2151 columns of SWIR). All data were collected on 2x2.5 cm sized sample cylinders, a scale at which the spatial coupling of the techniques is assured. These data are integrated by design, eliminating the need to downscale coarser measurements using assumptions, inferences, inversions, and interpolations. This scale consistent approach is critical to quantitative characterisation of mineral systems and has numerous applications to mineral exploration, such as linking alteration paragenesis with structural controls and petrophysical zonation.

Whilst the database is not 100% complete (i.e., it is missing data for some samples), it is, to our knowledge, the most complete dataset of its kind. It is a unique dataset which paves the way for a completely different approach to mineral exploration, to understanding mineral systems and to advancing the use of data analytics in the geosciences. Our team has extracted significant value out of this new integrated data as demonstrated by the examples contained herein. But we have only scratched the surface on the potential applications of this approach, and there is much to be revealed by the wider geoscience community. This data, associated imagery, modelling, and insights provide an optimal platform for further studies by providing comprehensive characterisation of the deposits, their footprints and host rocks. It describes a mineral system at the sample scale.

This project highlights the need to think carefully about how geoscience data is collected, and how collection and processing impact upon automated interpretation. The consistency of the scale, resolution and depth of investigation of input data are paramount and should be carefully considered in order to best capture geoscience data that is meaningful to data analytics. It is crucial to recognise that very few of the datasets utilised in geoscience (especially mineral exploration) are truly spatially coincident, truly quantitative (at all scales) or compatible (in terms of describing identical volumes). To make big data work in geosciences, changing how we approach the data will lead to improved outputs from data analytics, rather than the analytics themselves. Data must first be integrable to be integrated.

Ultimately, the most important aspects of data integration will always be tied to people. The integration of ideas and the linking of domain expertise is critical to align the mineral vectors provided by different techniques (Figure 28). Getting domain experts

https://doi.org/10.5194/essd-2023-464
Preprint. Discussion started: 20 February 2024

together in the field, core shed, laboratory and conference room is critical to developing improved methodologies for unlocking mineral potential and maximising the utility of data analytics. We hope this publication provides a platform for innovative research into this unique and complex mineral system and is a catalyst for adoption of this approach across mineral districts globally.

Competing interests

The contact author has declared that none of the authors has any competing interests

References

AGICO: AGICO Company Webpage. https://www.agico.com/text/products/jr6/jr6.php. Accessed 2022.

Allard, D., Comunian, A. and Renard, P.: Probability Aggregation Methods in Geoscience. Math Geosci 44, 545–581 https://doi.org/10.1007/s11004-012-9396-3, 2012.

Austin, J.R. and Blenkinsop, T.G.: The Cloncurry Lineament: geophysical and geological evidence for a deep crustal structure in the Eastern Succession of the Mount Isa Inlier. Precambr. Res. 163, 50–68, https://doi.org/10.1016/j.precamres.2007.08.012 2008.

Austin, J.R. and Blenkinsop, T.G.: Local to regional scale structural controls on mineralization and the importance of a major lineament in the eastern Mount Isa Inlier, Australia: Review and analysis with autocorrelation and weights of evidence. Ore Geol Rev, 35 (3-4), 298–316, https://doi.org/10.1016/j.oregeorev.2009.03.004, 2009.

Austin, J.R., Gazley, M.F., Patterson, B., leGras, M. and Walshe, J.L.: The Artemis Zn-Cu deposit: Integrated Petrophysical and Geochemical analyses. In: Uncover Cloncurry, Edited by Gazley, M., CSIRO, Australia, pp. 45, https://doi.org/10.4225/08/5858211087845, 2016a.

Austin, J.R., Walshe, J.L., Gazley, M.F., Sisson, M., leGras, M., Godel, B.: The Canteen Cu-Au prospect: Integrated Petrophysical and geochemical analyses. In: Uncover Cloncurry, Edited by Gazley, M., CSIRO, Australia, pp. 51, https://doi.org/10.4225/08/5858212d5c7de, 2016b.

Austin, J.R., Gazley, M.F, Godel, B., Hawkins, S., le Gras, M.: The Maronan Pb- Ag deposit: Integrated Petrophysical and Geochemical analyses. In: Uncover Cloncurry, Edited by Gazley, M., CSIRO, Australia, pp. 50. https://doi.org/10.4225/08/585820ef41b35, 2016c.

Austin, J. R., Gazley, M.F., Walshe, J.L., Godel, B., leGras, M, and Patterson, B.O.: The Monakoff Cu-Au-U deposit: Integrated Petrophysical and Geochemical analyses. In: Uncover Cloncurry, Edited by Gazley, M., CSIRO, Australia, pp. 50. https://doi.org/10.4225/08/585821240c01c, 2016d.

https://doi.org/10.5194/essd-2023-464
Preprint. Discussion started: 20 February 2024

Austin, J.R., Walshe, J.L., Gazley, M.F., Ibrahimi, T., Patterson, B.O., and leGras, M.: The Ernest Henry Cu-Au deposit: Integrated Petrophysical and Geochemical analyses. In: Uncover Cloncurry, Edited by Gazley, M., CSIRO, Australia, pp. 56. https://doi.org/10.4225/08/585820dc26de0, 2016e.

Austin, J.R. Gazley, M.F., Ibrahimi, T., Walshe, J.L., Patterson, B.O., and le Gras, M.: Uncover Cloncurry – The E1 North Cu-Au deposit: Integrated Petrophysical and geochemical analyses. In: Uncover Cloncurry, Edited by Gazley, M., CSIRO, Australia, pp. 50. https://doi.org/10.4225/08/585820bbc7223, 2016f.

Austin, J.R., Gazley, M.F., Walshe, J.L. and Patterson B.O.: Uncover Cloncurry – Summary: Integrated structural, metasomatic and metallogenic history of the Cloncurry District. CSIRO, Australia, pp. 45. https://doi.org/10.4225/08/5858208ac5528, 2016g.

Austin, J.R., Hawkins, Steph; Gazley, M.F., Patterson, B.O., leGras, M. and Walshe, J.: The Mount Colin Au-Cu deposit: Integrated petrophysical and geochemical analyses, CSIRO, Australia. https://doi.org/10.4225/08/585820d2990d3, 2016h.

Austin, J.R., Gazley, M.F., Patterson B.O., le Gras, M. and Walshe, J.: Uncover Cloncurry – The Cormorant Cu-Au Prospect: Integrated petrophysical and geochemical analyses. In: Uncover Cloncurry, Edited by Gazley, M., CSIRO, Australia. https://doi.org/10.4225/08/585820f9410a7, 2016i

Austin, J. R., Björk A. and Patterson, B.O.: Structural controls of the Ernest Henry IOCG deposit: Insights from integrated structural, geophysical and mineralogical analyses., ASEG Extended Abstracts, pp 1-5, https://doi.org/10.1080/22020586.2019.12073161, 2019.

Austin, J. R. and Patterson, B.O.: Deciphering deformation in ultramafic intrusions via magnetic fabric (AMS) and palaeomagnetic studies, Savannah Ni-PGE camp, NW Australia, Tectonophysics 793, https://doi.org/10.1016/j.tecto.2020.228608. 2020.

Austin, J. R.: Petrophysically constrained targeting of Iron Oxide Copper-Gold, Iron Sulphide Copper-Gold, Skarn and Broken Hill Type systems. CSIRO, Australia;. http://hdl.handle.net/102.100.100/429914?index=1, 2021a.

Austin, J.R: Mapping IOCG Fluid Pathways with Radiometrics: Case Studies, Tools and Exploration Strategy. CSIRO, Australia http://hdl.handle.net/102.100.100/435119?index=1, 2021b.

Austin, J. R., Birchall, R., Stromberg, J., Patterson, B., Bjork, A, Dhnaram, C., Lisitsin, V., Walshe, J. Gazley, M., leGras, M., Shelton, T., Spinks, S., Pearce, M., Schlegel, T., McFarlane, H. The Cloncurry METAL Geodatabase mk1: A scale-integrated relational geodatabase for Cloncurry District, Northwest Queensland. Brisbane, Qld: Geological Survey of Queensland; 2021. csiro: EP2021-0324. http://hdl.handle.net/102.100.100/429916?index=1. 2021a.

Austin, J. R., Patterson, B., Birchall, R., Björk, A., Walshe, J., Schlegel T., Stromberg, J., McFarlane, H., Shelton, T.D. and. Pearce, M.: Metasomatic controls on petrophysical zonation in IOCG mineral systems: An example from Ernest Henry,

Cloncurry District: Part III: Cloncurry METAL Final Report 2018/21, Edited by Austin, J., CSIRO Australia: http://hdl.handle.net/102.100.100/421957?index=1, 2021a

Austin, J. R., McFarlane, H. B., Schlegel, T. U., Patterson, B., Birchall, R., Walshe, J., Bjork, A., and Shelton, T. D.: Tectono-metasomatic history and structural controls of the Ernest Henry deposit: Insights from integrated mineralogy and magnetic fabric studies: Part IV: Cloncurry METAL final report 2018/2021. Edited by Austin, J., CSIRO, Australia pp 66: http://hdl.handle.net/102.100.100/429915?index=1, 2021b.

Austin, J.R., Schlegel, T.U., Walshe, J., Bjork, A. and Foss, C., Geophysical proxies for redox gradients in IOCG systems: Cloncurry District, Qld, Australia. Australian Society of Exploration Geophysicists Extended Abstracts, Volume 2021, 3rd Australasian Exploration Geoscience Conference, Brisbane, 2021. https://doi.org/10.5281/zenodo.7687590, 2021c.

Austin, J. R., Birchall, R., Stromberg, J., Patterson, B., Bjork, A, Dhnaram, C., Lisitsin, V., Walshe, J. Gazley, M., leGras, M., Shelton, T., Spinks, S., Pearce, M., Schlegel, T., McFarlane, H. The Cloncurry METAL Geodatabase mk1. The Geological Survey of Queensland (GSQ) Open Data Portal: https://geoscience.data.qld.gov.au/data/dataset/cr126168/resource/geo-doc1310615-cr126168, 2021d.

Bischof, L., Lagerstrom, R., Guo, Y., Huntington, J., and Mason, P.: An unmixing algorithm based on a large library of shortwave infrared spectra. CSIRO, Australia, pp 44. https://doi.org/10.4225/08/584c433f7ab79, 2011.

Biamonte, J., Wittek, P., Pancotti, N. et al. Quantum machine learning. Nature 549, pp 195–202. https://doi.org/10.1038/nature23474 , 2017.

Biedermann, A.R., Kunze, K., Zappone A. S. and Hirt, A. M.: Origin of magnetic fabrics in ultramafic rocks. IOP Conference Series: Materials Science and Engineering, Volume 82, 17th International Conference on Textures of Materials (ICOTOM 17), Dresden, Germany. https://doi:10.1088/1757-899X/82/1/012098, 2015.

Birchall, R., Austin, J.R., Stromberg, J.M., Schlegel, T.U., Shelton, T.D., Björk, A., Woodall, C.E. and McFarlane, H.B.: A revised alteration paragenesis for the Eloise Au-Cu deposit: Results of integrated TIMA mineralogy and hyperspectral studies. Part IX: Cloncurry METAL Final Report 2018/21, Edited by Austin, J., CSIRO, Australia pp 59: http://hdl.handle.net/102.100.100/433371?index=1, 2021.

Birchall, R. and Austin, J. R.: SEM-Based Mineral Mapping: a tool for unravelling metamorphic, metasomatic, metallogenic, and tectonic processes in the Cloncurry District. CSIRO, Australia. http://hdl.handle.net/102.100.100/445731?index=1. 2021.

Chadima, M. and Jelinek, V.: Anisoft 4.2: Anisotropy Data Browser for Windows. Agico, Inc. http://hdl.handle.net/11104/0163273, 2009.

https://doi.org/10.5194/essd-2023-464
Preprint. Discussion started: 20 February 2024

Chapman, L.H. and Williams, P.J.: Evolution of pyroxene–pyroxenoid–garnet alteration at the Cannington Ag–Pb–Zn Deposit, Cloncurry District, Queensland, Australia. Economic Geology 93, 1390–1405. https://doi.org/10.2113/gsecongeo.93.8.1390, 1998.

Clark, D. A.: Magnetic properties and magnetic signatures of the Trough Tank and Starra copper-gold deposits, Eastern Mount Isa Block. AMIRA Project 78/P96B: Applications of Rock magnetism. https://confluence.csiro.au/display/cmfr/Historic+Publications, 1988.

De Jong, G. and Williams, P.J.: Giant metasomatic system formed during exhumation of mid-crustal Proterozoic rocks in the vicinity of the Cloncurry Fault, Northwest Queensland. Australian Journal of Earth Sciences 42, pp 281–290. https://doi.org/10.1080/08120099508728202, 1995.

Ferré, E. C., Bordarier, C. and Marsh, J.S., 2002. Magma flow inferred from AMS fabrics in a layered mafic sill, Insizwa, South Africa, Tectonophysics 354, 1-23, ISSN 0040-1951, https://doi.org/10.1016/S0040-1951(02)00273-1.

Fitzpatrick, A.D.: Scale dependent electrical properties of sulphide deposits, PhD thesis, University of Tasmania, https://eprints.utas.edu.au/11546/9/Fitzpatrick_whole_thesis.pdf, 2006.

Gazley, M., Patterson, B., Austin, J., and Walshe, J.: Uncover Cloncurry - Osborne Cu-Au deposit: Integrated petrophysical and geochemical analyses. CSIRO, Australia, pp. 25. https://doi.org/10.4225/08/585820e576d1f, 2016a.

Gazley, M., Sisson, M., Austin, J.R., Patterson, B., le Gras, M. and Walshe, J.: The Trekelano Cu-Au deposit: Integrated petrophysical and geochemical analyses. In: Uncover Cloncurry, Edited by Gazley, M., CSIRO, Australia, 21 pp. https://doi.org/10.4225/08/5858211a8e914, 2016b.

Gazley, M., Sisson, M., Patterson, B., Austin, J.R., Walshe, J.: The Cameron River prospect: Integrated petrophysical and geochemical analyses. In: Uncover Cloncurry, Edited by Gazley, M., CSIRO, Australia. https://doi.org/10.4225/08/5aa17a27b1147, 2017.

Greiling, R. and Verma, P.: Strike-slip and tectonics granitoid emplacement: an AMS fabric study from the Odenwald Crystalline Complex, SW Germany. Mineralogy and Petrology 72: 165. https://doi.org/10.1007/s007100170032, 2001.

Gröger G., Kolbe T.H., Schmittwilken J, Stroh V, and Plümer L.: Integrating versions, history and levels-of-detail within a 3D geodatabase, in: Proceedings of the 1st international ISPRS/EuroSDR/DGPF-Workshop on Next Generation 3D City Models, edited by: Gröger G., Kolbe T.H., Bonn, June 21–22. EuroSDR, pp. 35–40, https://mediatum.ub.tum.de/1453849, 2005.

Haest, M., Cudahy, T., Laukamp, C. and Gregory, S.: Quantitative Mineralogy from Infrared Spectroscopic Data. I. Validation of Mineral Abundance and Composition Scripts at the Rocklea Channel Iron Deposits in Western Australia. Econ Geol, 107, 200-228, https://doi.org/10.2113/econgeo.107.2.209, 2012.

https://doi.org/10.5194/essd-2023-464
Preprint. Discussion started: 20 February 2024

Hitzman, M.W., Oreskes, N. and Einaudi, M.T.: Geological characteristics and tectonic setting of Proterozoic iron oxide (Cu-U-Au-REE) deposits. Precamb. Res., 58: pp 241-287. https://doi.org/10.1016/0301-9268(92)90121-4, 1992.

Hrouda, F., Faryad, S.W., Franěk, J. and Chlupáčová, M.: Magnetic fabrics in garnet peridotites–pyroxenites and host felsic granulites in the South Bohemian Granulites (Czech Republic): Implications for distinguishing between primary and metamorphism induced fabrics. Gondwana Res 23, 956-972, https://doi.org/10.1016/j.gr.2012.05.020, 2013.

Jelinek, V.: Characterization of the magnetic fabric of rocks. Tectonophysics 79, 63–67. https://doi.org/10.1016/0040-1951(81)90110-4, 1981.

Kent, J., Briden, J., and Mardia, K.: Linear and planar structure in ordered multivariate data as applied to progressive demagnetization of palaeomagnetic remanence: Geophys J Int 75, 593-621, https://doi.org/10.1111/j.1365-246X.1983.tb05001.x, 1983.

Knight, M.D. and Walker, G.P.: Magma flow directions in dikes of the Koolau Complex, Oahu, determined from magnetic fabric studies. J Geophys Res: Solid Earth, 93(B5), 4301-4319, https://doi.org/10.1029/JB093iB05p04301, 1988.

Knorsch, M., Deditius, A.P., Xia, F., Pearce, M.A. and Uvarova, Y: The impact of hydrothermal mineral replacement reactions on the formation and alteration of carbonate-hosted polymetallic sulfide deposits: A case study of the Artemis prospect, Queensland, Australia. Ore Geology Reviews, 116, p.103232 https://doi.org/10.1016/j.oregeorev.2019.103232, 2020.

Lambourn, S.S. and Shelley, E.P.: Cloncurry detailed airborne magnetic and radiometric survey, Queensland 1970. Record 1972/110. Geoscience Australia, Canberra. http://pid.geoscience.gov.au/dataset/ga/12791, 1972.

Laukamp, C., Mason, P., Lau, I., Warren, P. and Rodger, A.: A mineral dataset for testing methods of SWIR interpretation. CSIRO EP175248, 10p, https://doi.org/10.25919/5f1f243e51b33, 2017.

Laukamp, C., Rodger, A., LeGras, M., Lampinen., H., Lau, I., Pejcic. B., Stromberg, J., Francis, N. and Ramanaidou, E.: Mineral Physicochemistry Underlying Feature-Based Extraction of Mineral Abundance and Composition from Shortwave, Mid and Thermal Infrared Reflectance Spectra. Minerals. 11, 347, https://doi.org/10.3390/min11040347, 2021.

Lee, D. and Seung, H.: Learning the parts of objects by non-negative matrix factorization. Nature 401, 788–791 https://doi.org/10.1038/44565. 1999.

Lowrie W. 1997. Fundamentals of Geophysics. Cambridge University Press xiv, 354 pp

Lypaczewski,P., Rivard, B.: Estimating the Mg# and AlVI content of biotite and chlorite from short wave infrared reflectance spectroscopy: Predictive equations and recommendations for their use. International Journal of Applied Earth Observation. 68, 116-126, 2018.

https://doi.org/10.5194/essd-2023-464
Preprint. Discussion started: 20 February 2024

McFarlane, H. B., Bjork, A., Stromberg, J., Austin, J. R., Birchall, R. Schlegel, T. U. and Shelton, T. D. Patterson, B.: Mineralogical, petrophysical and structural characterisation of Osborne Cu-Au deposit: Part IIX: Cloncurry METAL Final Report 2018/2021, Edited by Austin, J., CSIRO, Australia, pp 53: http://hdl.handle.net/102.100.100/433817?index=1, 2021a.

McFarlane, H. B., Austin, J. R., Schlegel, T. U., Birchall, R, Bjork, A., Stromberg, J., Walshe, J., Shelton, T, and Pearce, M.: Starra 276 and 251: Redox Gradients and Structural Controls - Integrated petrophysical, structural and mineralogical analysis: Part V: Cloncurry METAL Final Report 2018/2021. Edited by Austin, J., CSIRO, Australia. http://hdl.handle.net/102.100.100/429198?index=1, 2021b.

McFarlane, H.B. and Austin, J.R.: Anisotropy of Magnetic Susceptibility (AMS): A powerful tool for quantifying IOCG structural controls and predicting ore body geometries. CSIRO, Australia. 2021.

Patterson, B., Gazley, M., Austin, J.R. and Walshe, J.: The Merlin Mo-Re deposit: Integrated petrophysical and geochemical analyses In: Uncover Cloncurry, Edited by Gazley, M., CSIRO, Australia, 30 pp. https://doi.org/10.4225/08/585821367807e, 2016a.

Patterson, B., Austin, J.R., Gazley, M. and Walshe, J.: The SWAN Cu-Au deposit: Integrated petrophysical and geochemical analyses. In: Uncover Cloncurry, Edited by Gazley, M., CSIRO, Australia. https://doi.org/10.4225/08/5858209427c32, 2016.

Pearce, Mark; Austin, Jim; McFarlane, Helen; Birchall, Renee; Spinks, Sam. Cloncurry METAL Final Report Part VII: Cloncurry METAL Final Report 2018/2021, Edited by Austin, J., CSIRO, Australia pp 46: http://hdl.handle.net/102.100.100/429788?index=1 2021.

Roache, T. J. Williams, P.J., Richmond J. M. and Chapman, L.H.: Vein and Skarn Formation at the Cannington Ag–Pb–Zn Deposit, northeastern Australia. The Canadian Mineralogist Vol. 43, pp. 241-262, 2005.

Riisager, P., Abrahamsen, N.: Palaeomagnetic errors related to sample shape and inhomogeneity. Earth Planets Space (55), 83-91, 2003.

Rubenach, M.J. and Barker, A.J.: Metamorphic and metasomatic evolution of the Snake Creek Anticline, Eastern Succession, Mt Isa Inlier. Geological framework and mineralisation in the Mt Isa Eastern Succession, Northwest Queensland. Aust J Earth Sci 45, 363–372, 1998.

Rubenach M.: Structural Controls of Metasomatism on a Regional Scale. In: Metasomatism and the Chemical Transformation of Rock. Lecture Notes in Earth System Sciences. Springer, Berlin, Heidelberg, 2013.

Rybach, L.: Radioactive heat production in rocks and its relation to other petrophysical parameters. Pure Appl. Geophys., 114, 309–318, 1976.

Rybach, L.: Determination of heat production rate. In Handbook of Terrestrial Heat Flow Density Determination, ed. R. Haenel, L. Rybach and L. Stegena, Dordrecht: Kluwer Academic Publishers, p. 486, 1988.

Ryan, C.G., Siddons, D.P., Kirkham, R., Li, Z.Y., De Jonge, M.D., Paterson, D.J., Kuczewski, A., Howard, D.L., Dunn, P.A., Falkenberg, G. and Boesenberg, U.: Maia X-ray fluorescence imaging: Capturing detail in complex natural samples. In Journal of Physics: Conference Series (Vol. 499, No. 1, p. 012002). IOP Publishing, 2014.

Schlegel T.U., Birchall R., Stromberg J.M., McFarlane H., Shelton T., Godel B., Bjork A., Pearce M.A., Walshe J.L., and Austin J. (2021). Mineral System Knowledge via Integration of Mineralogy, Geochemistry and Petrophysics - A case study on the Ernest Henry IOCG deposit. Part II: Cloncurry METAL final report 2018/2021. Edited by Austin, J., CSIRO, Australia pp 46:. CSIRO, Australia.

Schlegel, T.U.: Mapping Mineral Zonation using Integrated TIMA Mineralogy and Geochemistry: Vectoring to Grade. CSIRO, Australia, pp 8. http://hdl.handle.net/102.100.100/433707?index=1, 2021.

Schlegel T.U., Birchall R., Shelton T.D., Austin J.R.: Mapping the mineral zonation at the Ernest Henry iron oxide copper-gold deposit: Vectoring to Cu-Au mineralization using modal mineralogy. Econ Geol, 117, pp. 485 – 494. DOI:10.5382/ECONGEO.4915, 2022.

Schmidt, P.W., McEnroe, S.A., Clark, D.A. and Robinson, P.: Magnetic properties and potential field modeling of the Peculiar Knob metamorphosed iron formation, South Australia: An analog for the source of the intense Martian magnetic anomalies?. J Geophys Res: Solid Earth, 112(B3), 2007.

Schodlok, M.C., Whitbourn, L., Huntington, J., Mason, P., Green, A., Berman, M., Coward, D., Connor, P., Wright, W., Jolivet, M. and Martinez, R.: HyLogger-3, a visible to shortwave and thermal infrared reflectance spectrometer system for drill core logging: functional description. Aust J Earth Sci, 63(8), pp.929-940, 2016.

Siddons, D.P., Kirkham, R., Ryan, C.G., De Geronimo, G., Dragibem A., Kuczewski, A.J., Li, Z.Y., Carini, G., Pinelli, D., Beuttenmuller, R., Elliot, D., Pfeffer, D., Tyson, T.A, Moorhead, G.F. and Dun, P.A.: A Maia X-ray microprobe detector array system. Journal of Physics: Conference Series, 2014.

Sonntag, I., Laukamp, C., Hagemann, S.G.: Low potassium hydrothermal alteration in low sulfidation epithermal systems as detected by IRS and XRD: An example from the Co-O mine, Eastern Mindaneo, Phillipines. Ore Geol Rev, 45, 47-60, 2012.

Torsvik, T. H., Sturt, B. A., Swensson, E., Andersen, T. B. and Dewey, J. F.: Palaeomagnetic dating of fault rocks: evidence for Permian and Mesozoic movements and brittle deformation along the extensional Dalsfjord Fault, western Norway. Geophys J Int 109: 565-580. doi:10.1111/j.1365-246X.1992.tb00118.x,1992.

Walshe, J. L., Cooke, D. R., Neumayr, P.: Five questions for fun and profit: A mineral system perspective on metallogenic epochs, provinces and magmatic hydrothermal Cu and Au deposits. In: Mao, J., Bierlein, F.P. (eds) Mineral Deposit Research: Meeting the Global Challenge. Springer, Berlin, Heidelberg. https://doi.org/10.1007/3-540-27946-6_124, 2005.

https://doi.org/10.5194/essd-2023-464
Preprint. Discussion started: 20 February 2024

Walshe J. L., Gazley M. F., Austin J. R., Patterson B. O.: Chemical gradients in the Cloncurry Mineral System: Vectors to grade? In: Uncover Cloncurry, Edited by Gazley, M., CSIRO, Australia. https://doi.org/10.4225/08/585820a819235, 2016.

Williams, M. J., Schlegel, T. U., Austin, J., Lisitsin, V., Francis, N., Armstrong, D., Wathen-Dunn, K., Dhnaram, C.: Signatures of Key Mineral Systems in the Eastern Mount Isa Province, Queensland: New Perspectives from Data Analytics. CSIRO, Australia: pp109 https://doi.org/10.25919/gv7t-xr02, 2022

Williams, P.J. and Heinemann, M.: Maramungee; a Proterozoic Zn skarn in the Cloncurry District, Mount Isa Inlier, Queensland, Australia. Econ Geol 88, 1114–1134, https://doi.org/10.2113/gsecongeo.88.5.1114, 1993.

Williams, P.J. and Baker, T.: Regional-scale association of Skarn alteration and base metal deposits in the Cloncurry District, Mount Isa Inlier, Queensland, Australia. Transactions of the Institute of Mining and Metallurgy Section B (Applied Earth Science) 104, 189–192, https://minabs.americangeosciences.org/vufind/Record/2001069649, 1995.

Williams, P. J., Pendergast, W. J. and Dong, G.: Late orogenic alteration in the wall rocks of the Pegmont Pb–Zn deposits, Cloncurry District, Queensland, Australia. Econ Geol 93, 1180–1189, https://doi.org/10.2113/gsecongeo.93.8.1180, 1998.

Závada, P., Calassou, T., Schulmann, K., Hrouda, F., Štípská, P., Hasalová, P., Míková, J., Magna, T. and Mixa, P.: Magnetic fabric transposition in folded granite sills in Variscan orogenic wedge. J Struct Geol. 94, 166–183, https://doi.org/10.1016/j.jsg.2016.11.007, 2017.

https://doi.org/10.5194/essd-2023-464
Preprint. Discussion started: 20 February 2024

Open Access Earth System Science Data Discussions

Figures

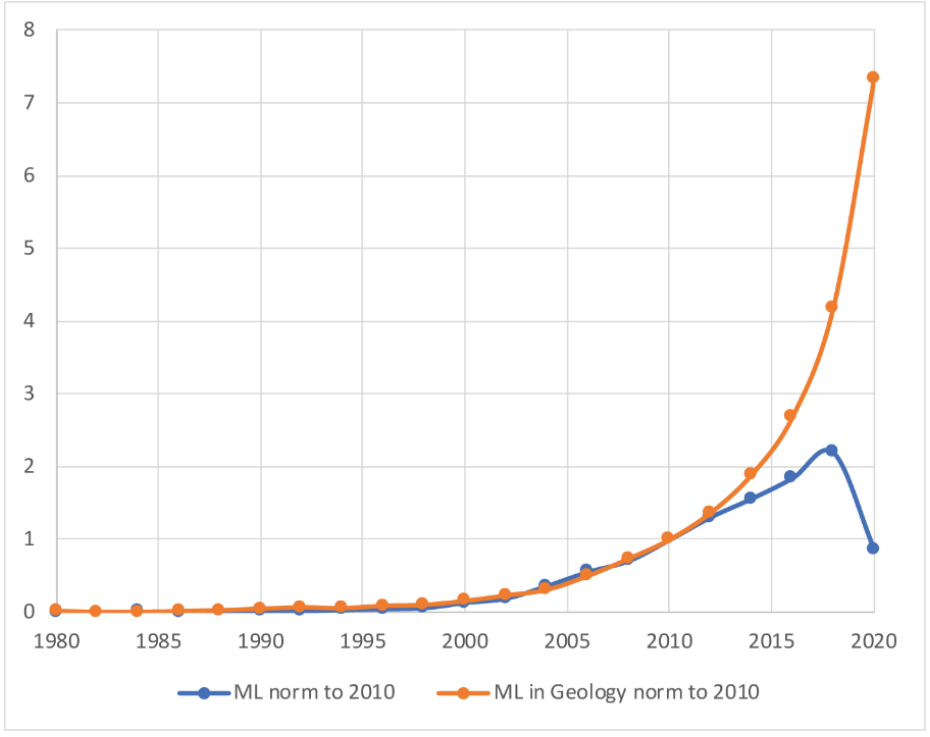

Figure 1: Results of Google Scholar™ search for the phrase "Machine Learning" vs results for the phases "Machine Learning" and geology. Data for each point on the graph comprises all result for the 2 years prior. Both datasets are normalised to the start of 2010, which is where the trends diverge. From Austin et al., 2021a.

https://doi.org/10.5194/essd-2023-464
Preprint. Discussion started: 20 February 2024

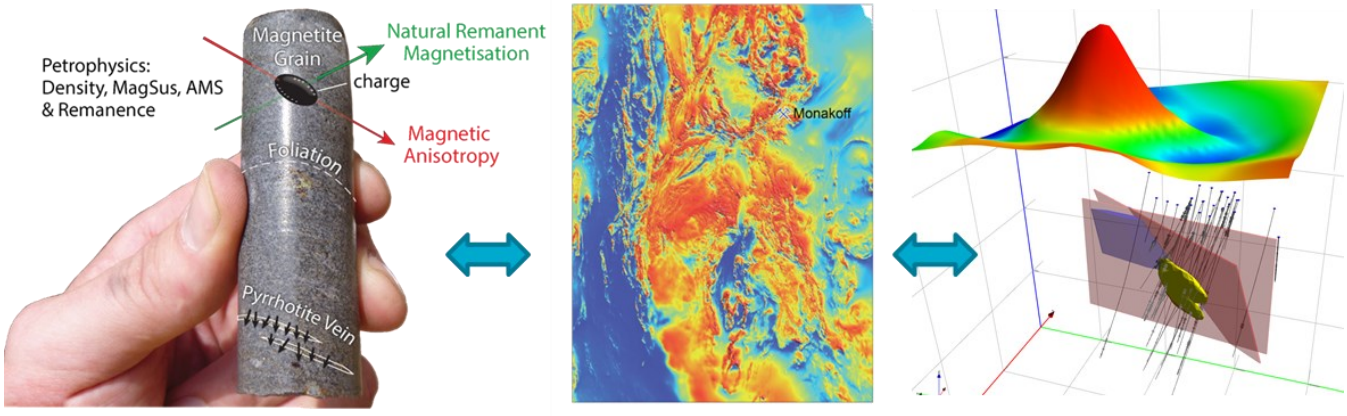

Figure 2: Illustration of some of the different scales of data and observation in mineral exploration. A. is the sample scale use for this project and should be considered the optimal scale at which geoscience can be meaningfully integrated. Integrated petrophysics can be used to constrain regional scale geophysical interpretations (B) and camp/deposit scale studies (C). Pane C also illustrates the multi-dimensional nature of geoscience.

https://doi.org/10.5194/essd-2023-464
Preprint. Discussion started: 20 February 2024

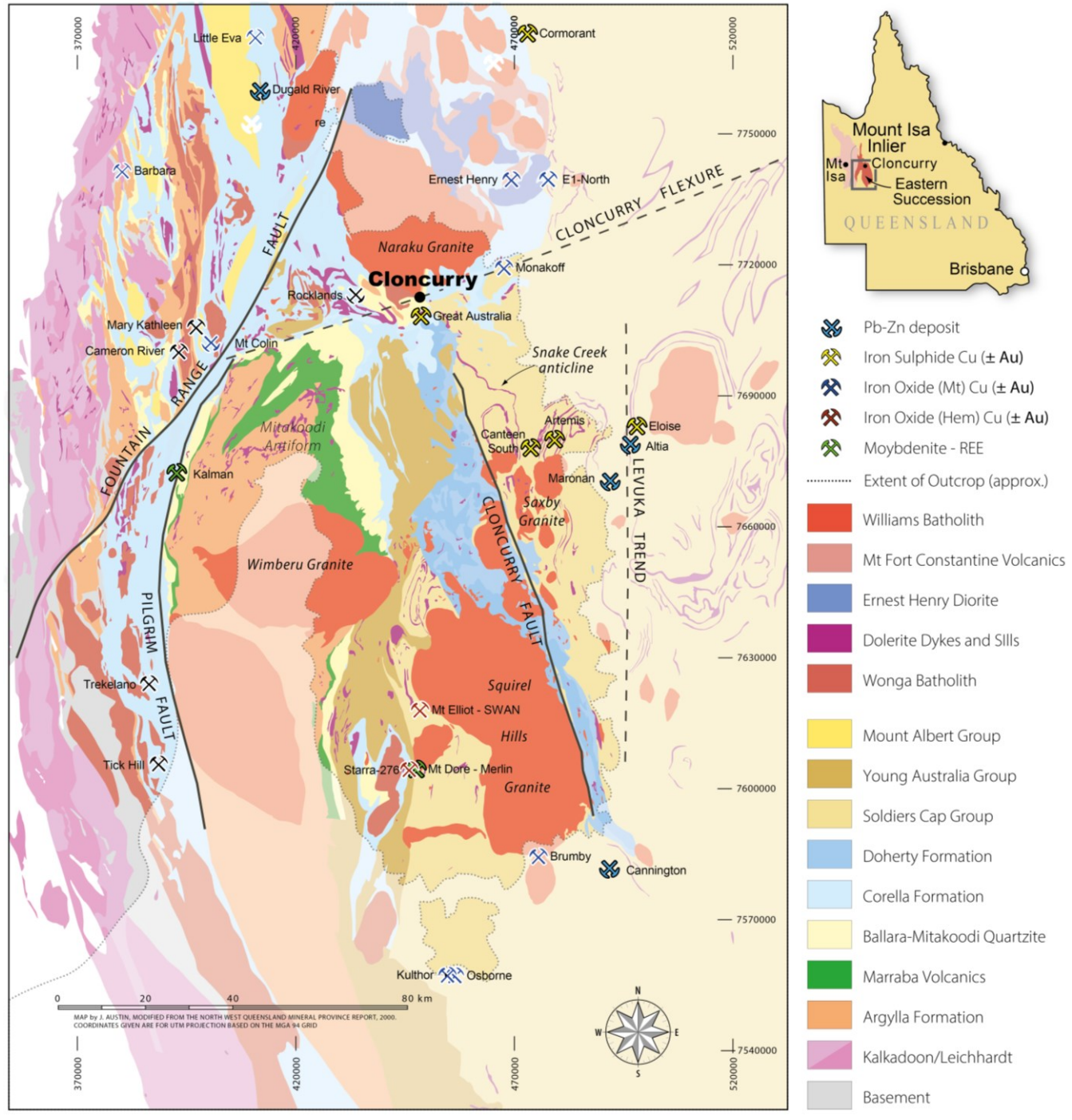

Figure 3: Geological map of the Cloncurry District with deposits from which samples in the database were taken. Modified from Austin and Blenkinsop, 2008.

https://doi.org/10.5194/essd-2023-464
Preprint. Discussion started: 20 February 2024

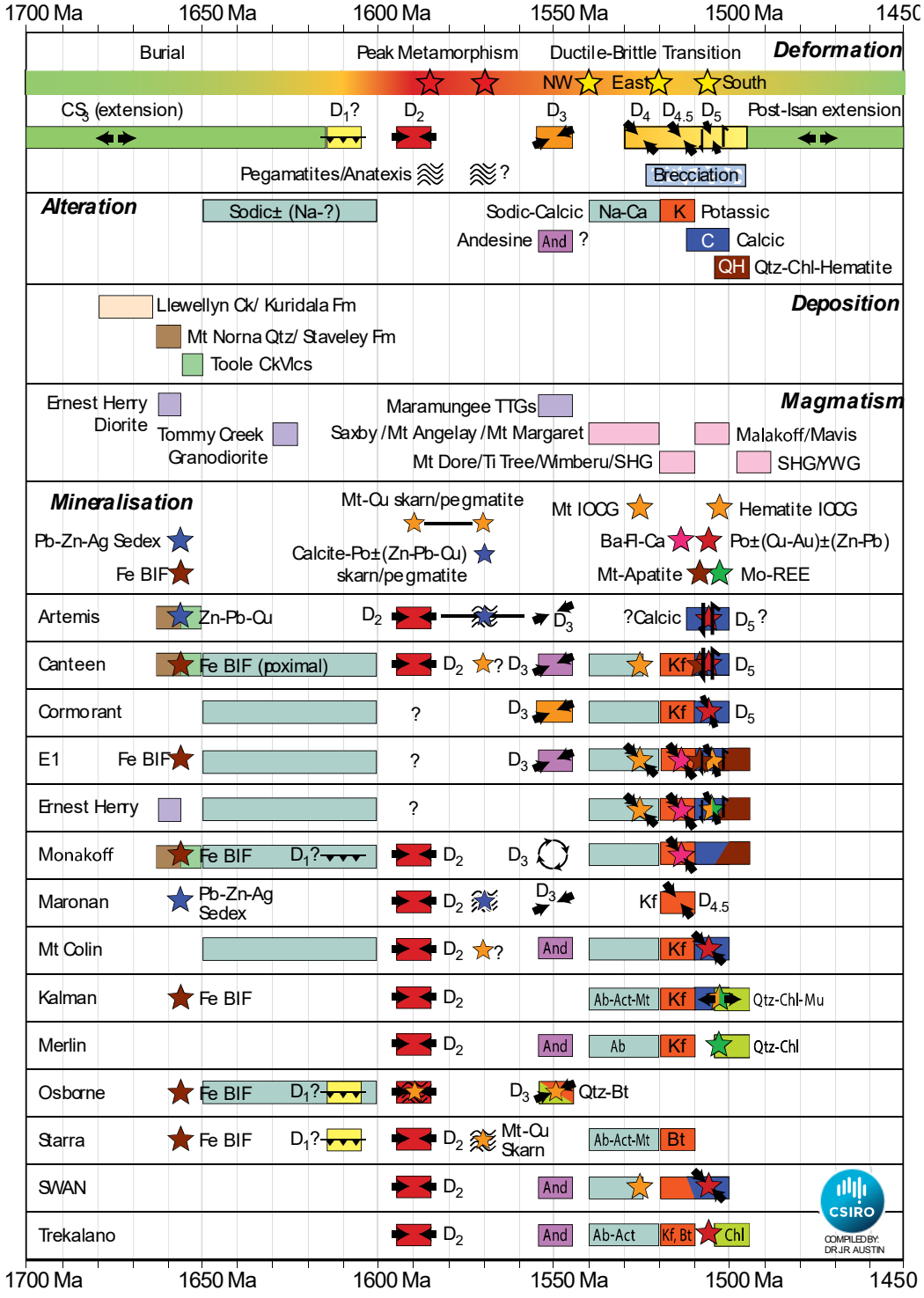

Figure 4: Condensed tectonic, metasomatic and metallogenic history of the Cloncurry District mineral system, and the processes that occurred at each of the deposits and prospects discussed in the study (from Austin et al., 2016g).

https://doi.org/10.5194/essd-2023-464
Preprint. Discussion started: 20 February 2024

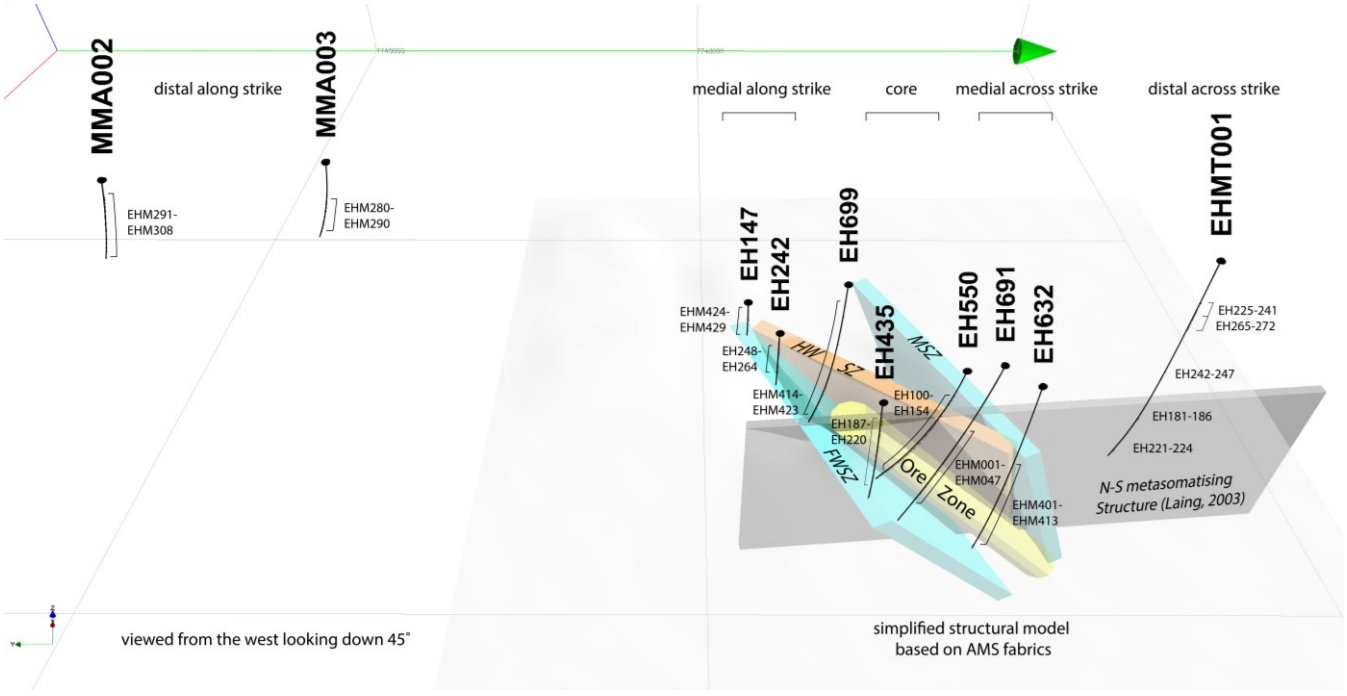

Figure 5: Simplified 3-D structural model of Ernest Henry based on measured AMS fabrics. All drill holes sampled are presented along with the respective sample numbers. The zonation of the system as it related to the samples is approximated by titles along the top of the figure. Model is viewed from the west and looking down at ~45˚. Scale varies in this perspective view.

https://doi.org/10.5194/essd-2023-464
Preprint. Discussion started: 20 February 2024

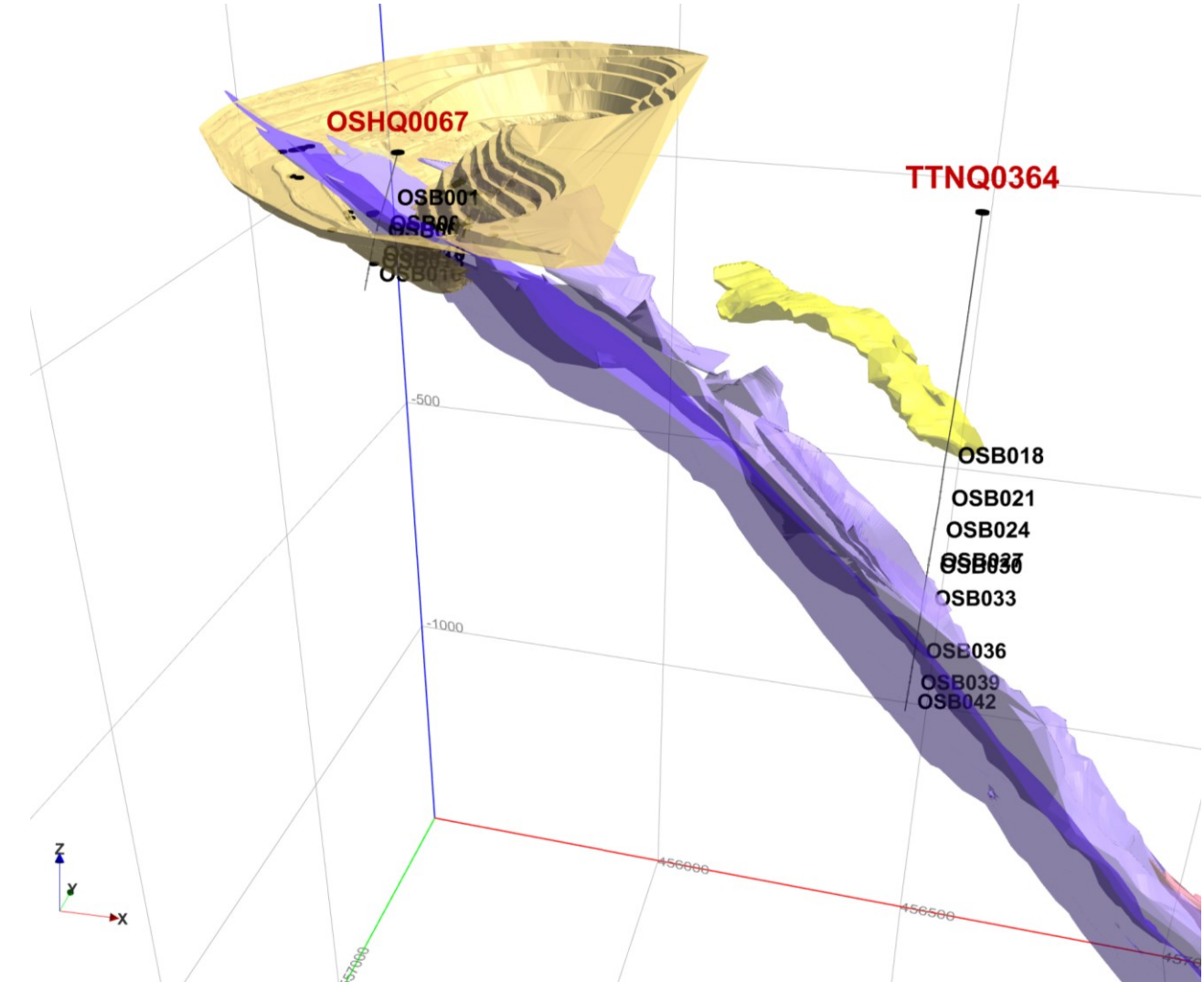

Figure 6: Sampling coverage of Osborne drill holes relative to the ENE dipping mineralised body (in purple).

https://doi.org/10.5194/essd-2023-464
Preprint. Discussion started: 20 February 2024

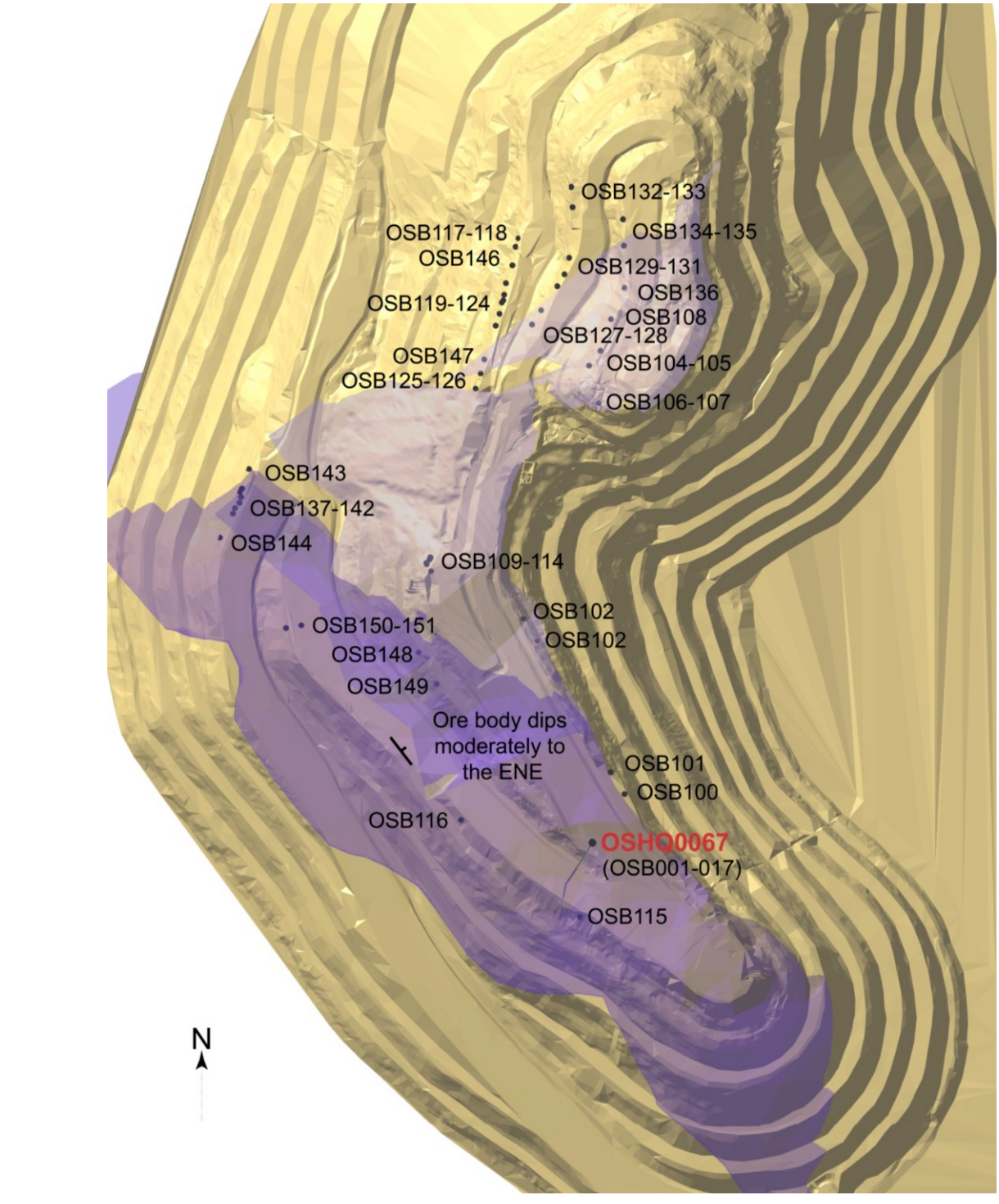

1170 **Figure 7: Sampling coverage of the Osborne open pit. The approximate position of the ENE dipping mineralised body is shown in purple. Note that the body is 3D, continuing underground in the deepest parts of the pit in the ENE.**

https://doi.org/10.5194/essd-2023-464
Preprint. Discussion started: 20 February 2024

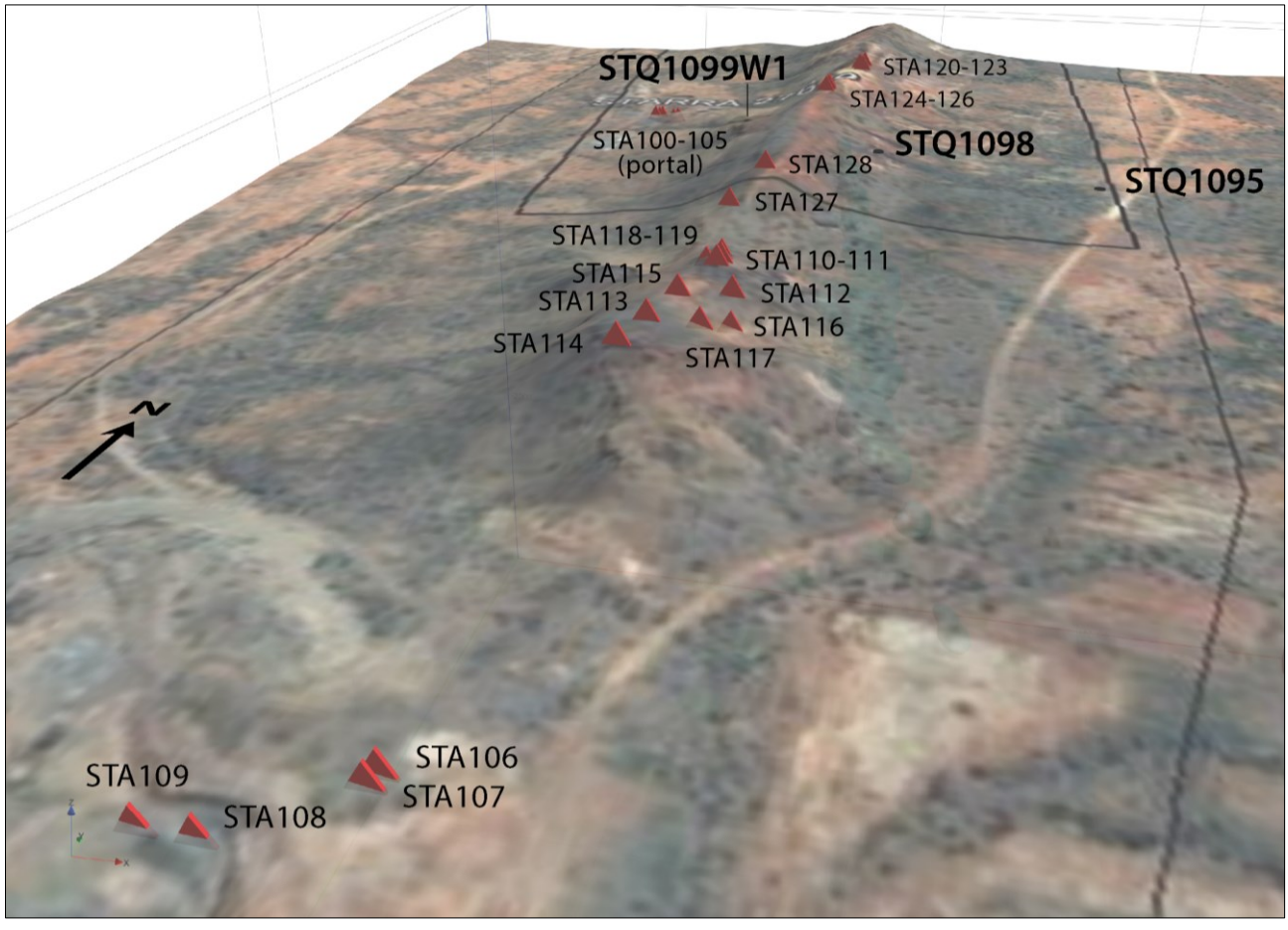

Figure 8: 3D view of GoogleEarth™ imagery draped on a DEM over an ironstone ridge cropping out between Starra-257 and Starra-276. The majority of surface samples were oxidised (i.e., Hematite-dominant) ironstones which we will use to examine the relationships between redox and mineral zonation along strike using TIMA and pXRF.

https://doi.org/10.5194/essd-2023-464
Preprint. Discussion started: 20 February 2024

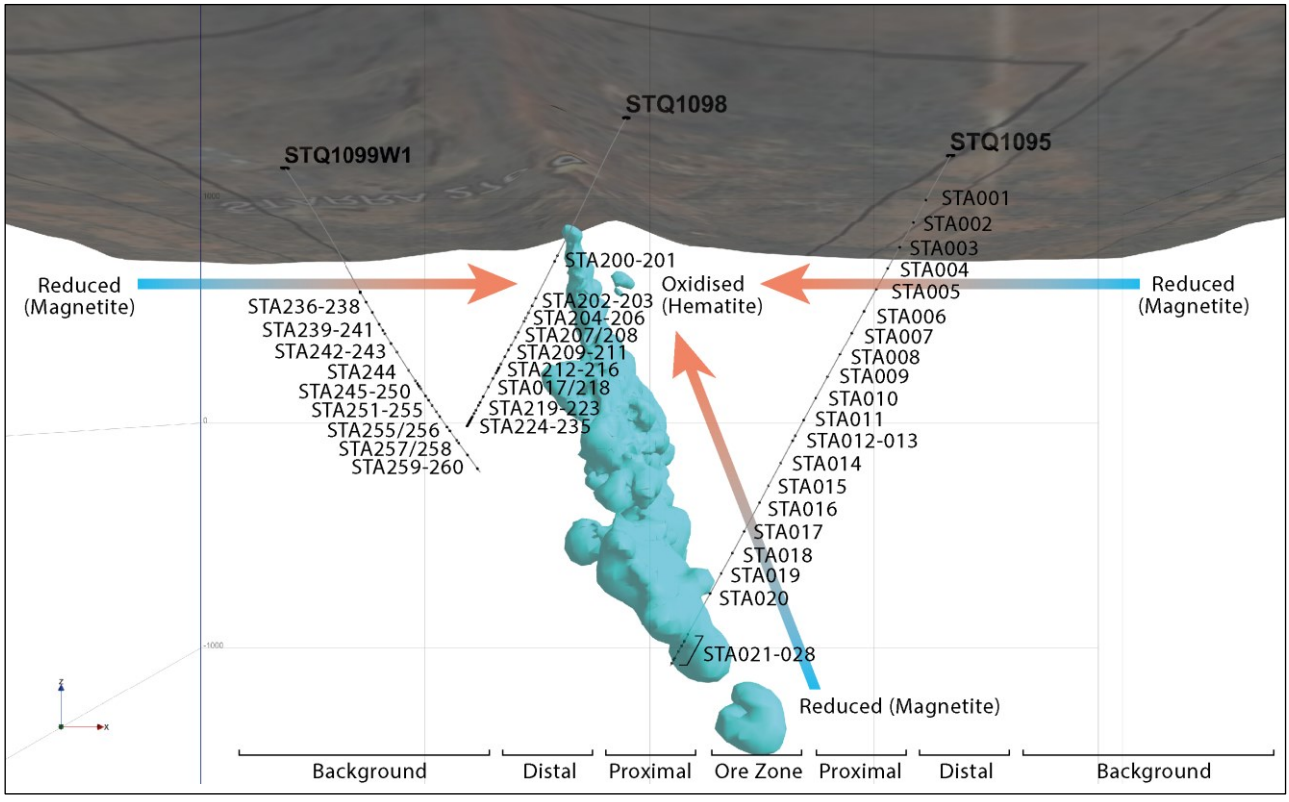

Figure 9: 3D view of GoogleEarth™ imagery draped on a DEM above Starra-276, and the location of samples. The turquoise body is a 0.75% equivalent copper grade shell. Underground sampling provides excellent east to west and top to bottom coverage across the Starra system and will allow us to garner insights into the relationships between redox and mineralisation using TIMA and pXRF.

https://doi.org/10.5194/essd-2023-464
Preprint. Discussion started: 20 February 2024

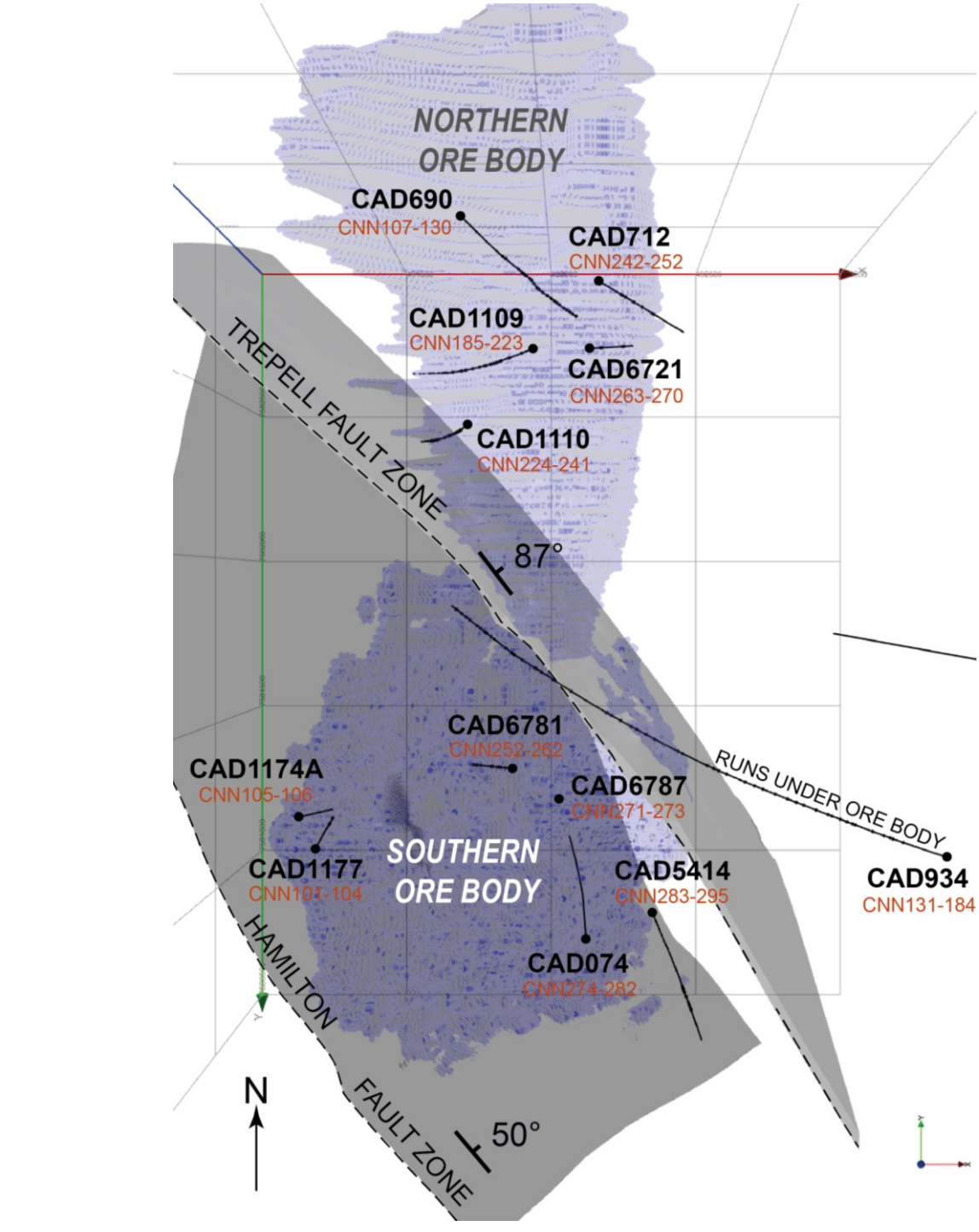

Figure 10: 3D Model of the Cannington ore body, with samples obtained during the January Field trip. Sampling covers the northern and southern mineralised zones (including all seven ore types), the alteration zone adjacent to the ore body and the background lithologies (including: psammite, schist, gneiss and amphibolite).

https://doi.org/10.5194/essd-2023-464
Preprint. Discussion started: 20 February 2024

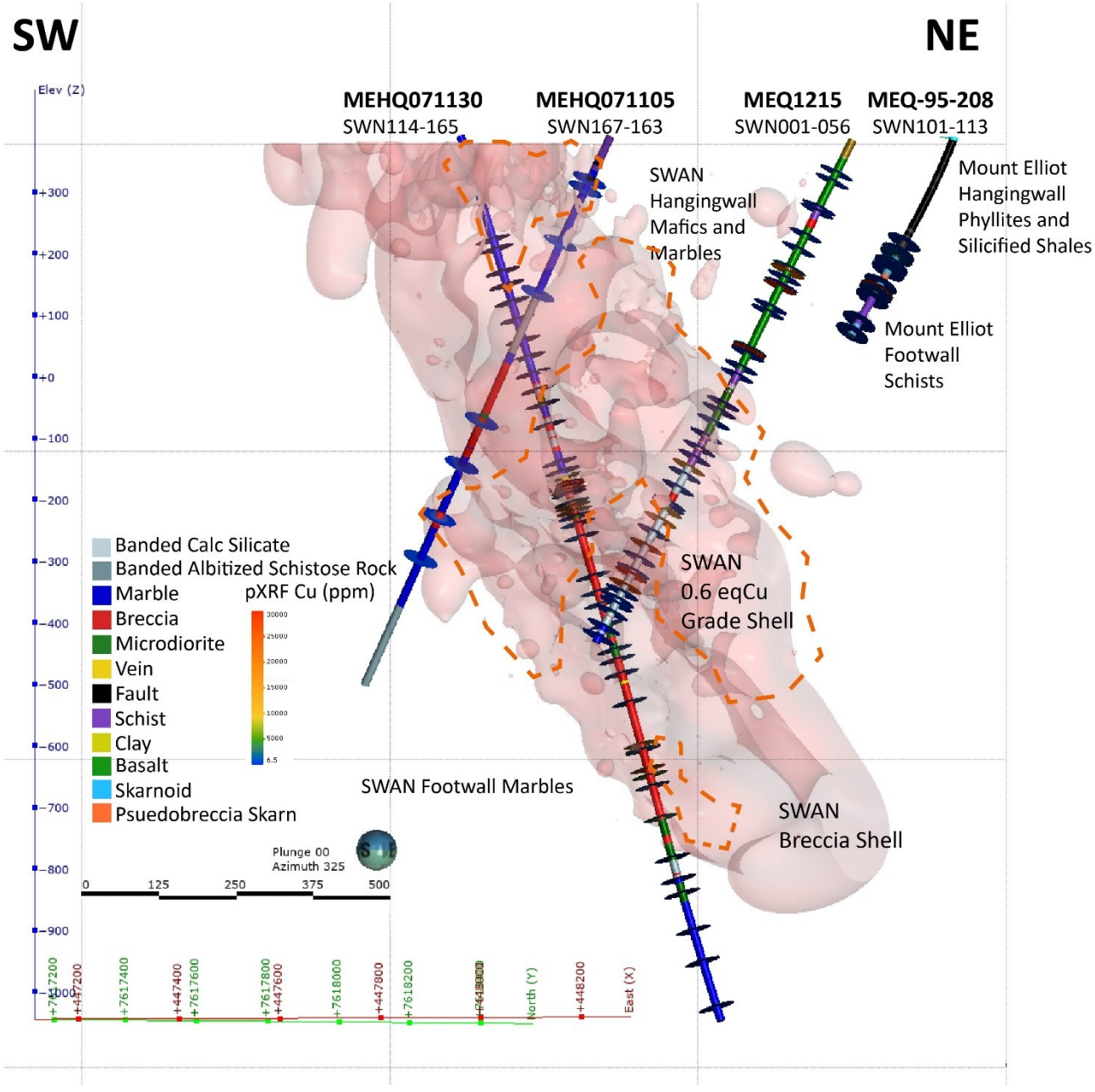

Figure 11: Sample coverage of the SWAN-Mount Elliot mineral systems with the drillholes, logging, and sample density (with pXRF results) with respect to the breccia and 0.6 eq Cu grade shells modelling from the Chinova Drillhole database in Leapfrog Geo, which plunges to the North at ~70°.

https://doi.org/10.5194/essd-2023-464
Preprint. Discussion started: 20 February 2024

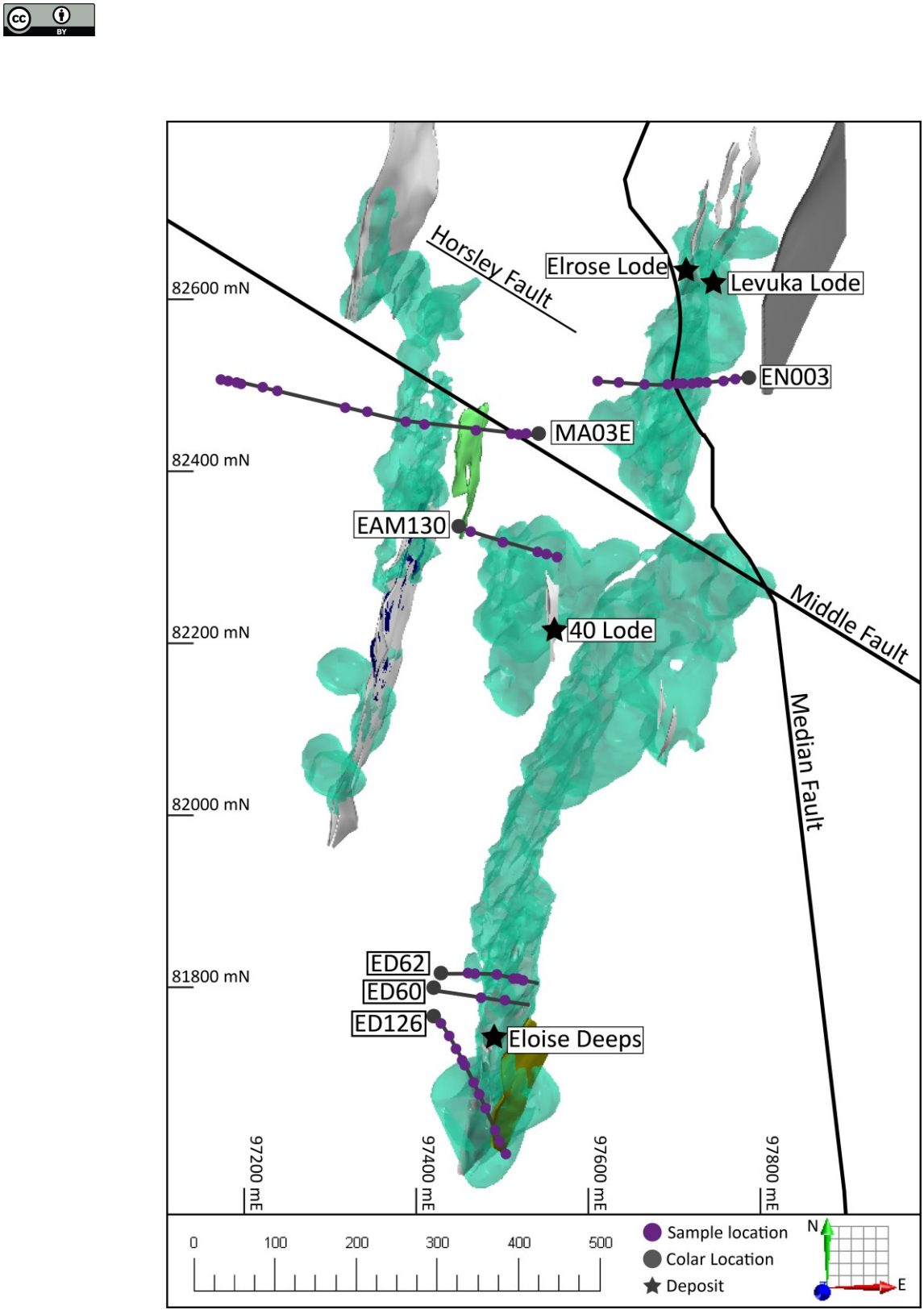

Figure 12: Sampled extent of the Eloise system, viewed from above, with the drillholes intersected, and sample density with respect to the various ore bodies (labelled), which are based on Leapfrog™ grade interpolations in the SMI Eloise Digital Data Atlas.

https://doi.org/10.5194/essd-2023-464
Preprint. Discussion started: 20 February 2024

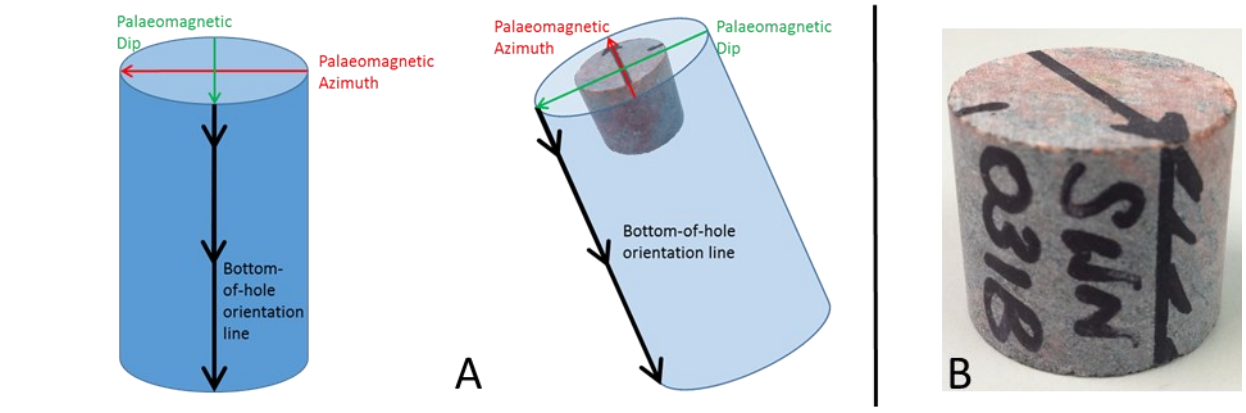

1195

Figure 13: A) Diagram of palaeomagnetic sample orientation mark-up procedure for oriented diamond core; B) Fully prepared palaeomagnetic sample including AMS mark-up.

https://doi.org/10.5194/essd-2023-464
Preprint. Discussion started: 20 February 2024

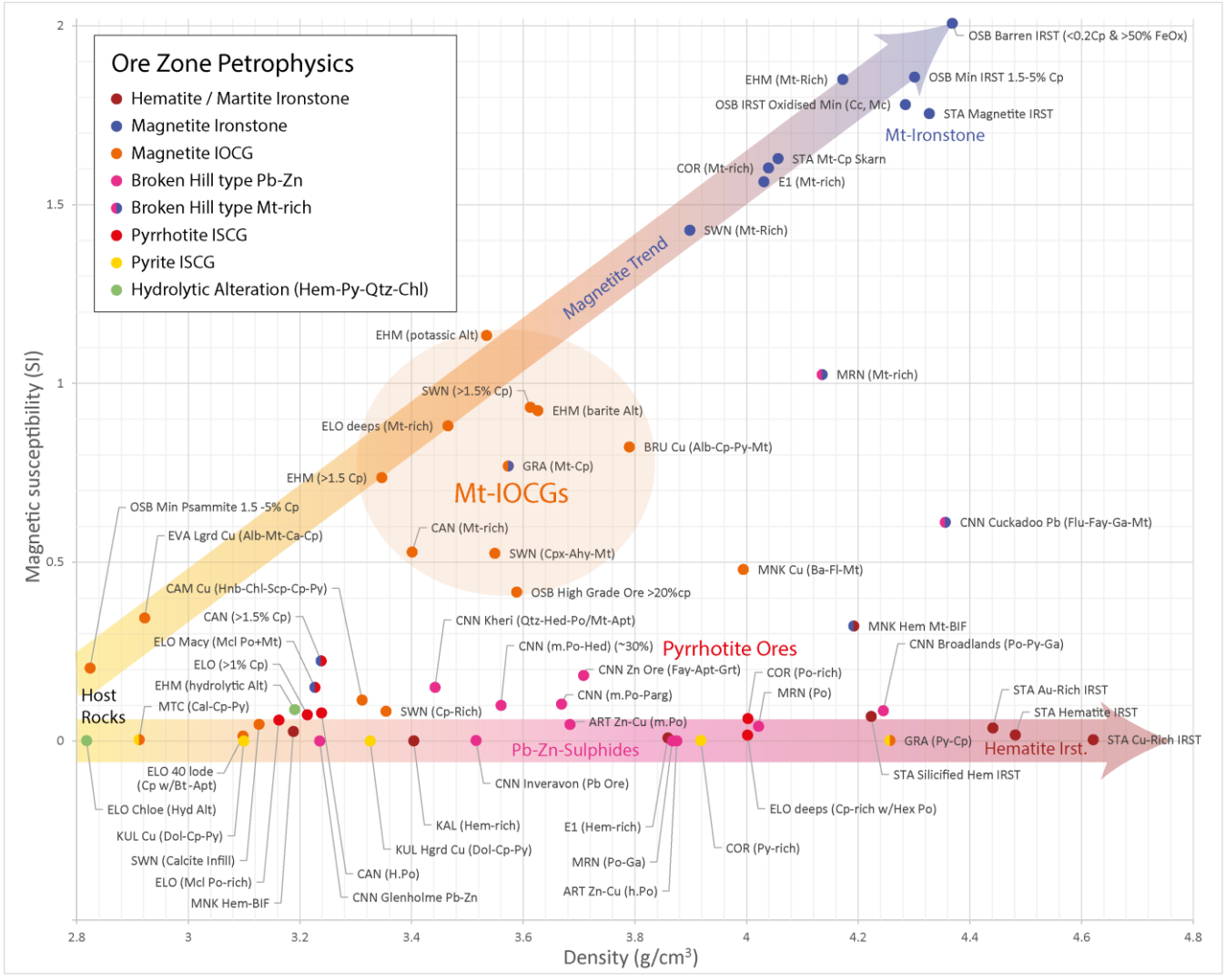

Figure 14: Plotting density vs magnetic susceptibility data are a common method for differentiating the abundances of major ore forming minerals, e.g., hematite, magnetite and pyrrhotite, providing knowledge that can be used to constrain geophysical inversions, but also insights into the chemical factors controlling mineralisation, such as redox (Austin, 2021 b,c). Figure from Austin, 2021a.

https://doi.org/10.5194/essd-2023-464
Preprint. Discussion started: 20 February 2024

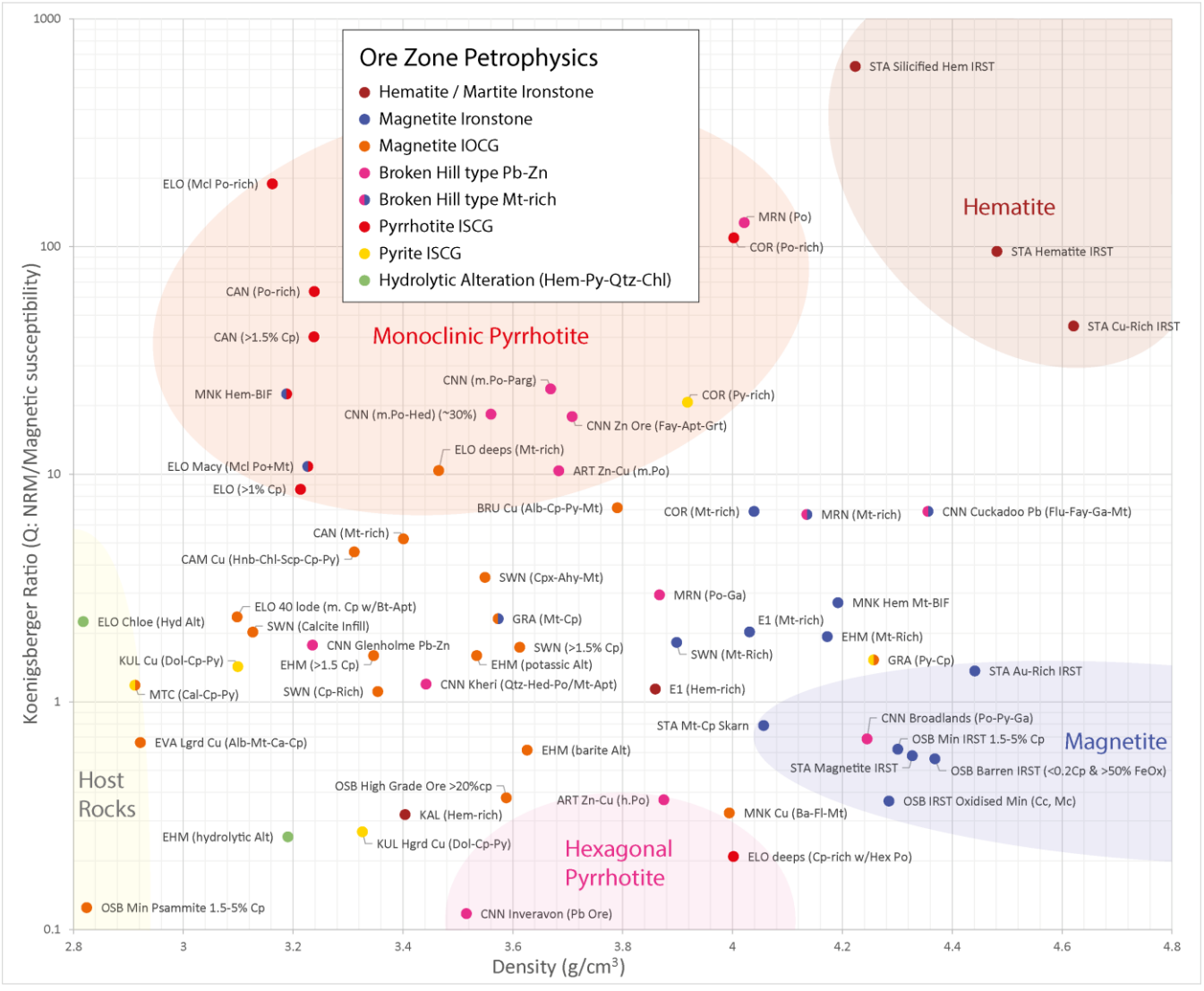

Figure 15: Koenigsberger ratio (J:K) plotted relative to density is one tool Petrophysicists use to characterise the dominant magnetic minerals within deposits and their footprints. Fe oxides and sulphides such as hematite, magnetite and monoclinic pyrrhotite all have characteristic petrophysical properties which provide information about the chemical conditions leading to mineralisation (e.g, redox and or pH). Figure from Austin, 2021a.

https://doi.org/10.5194/essd-2023-464
Preprint. Discussion started: 20 February 2024

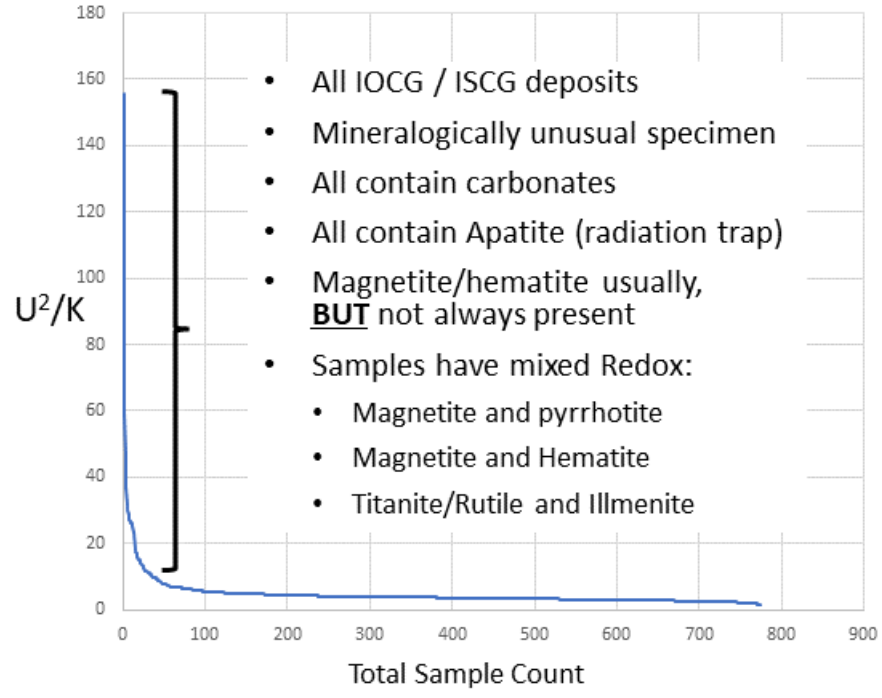

Figure 16: A plot of U^2/K sorted from high –to- low suggests that U anomalism is associated with characteristic mineralogical properties.

https://doi.org/10.5194/essd-2023-464
Preprint. Discussion started: 20 February 2024

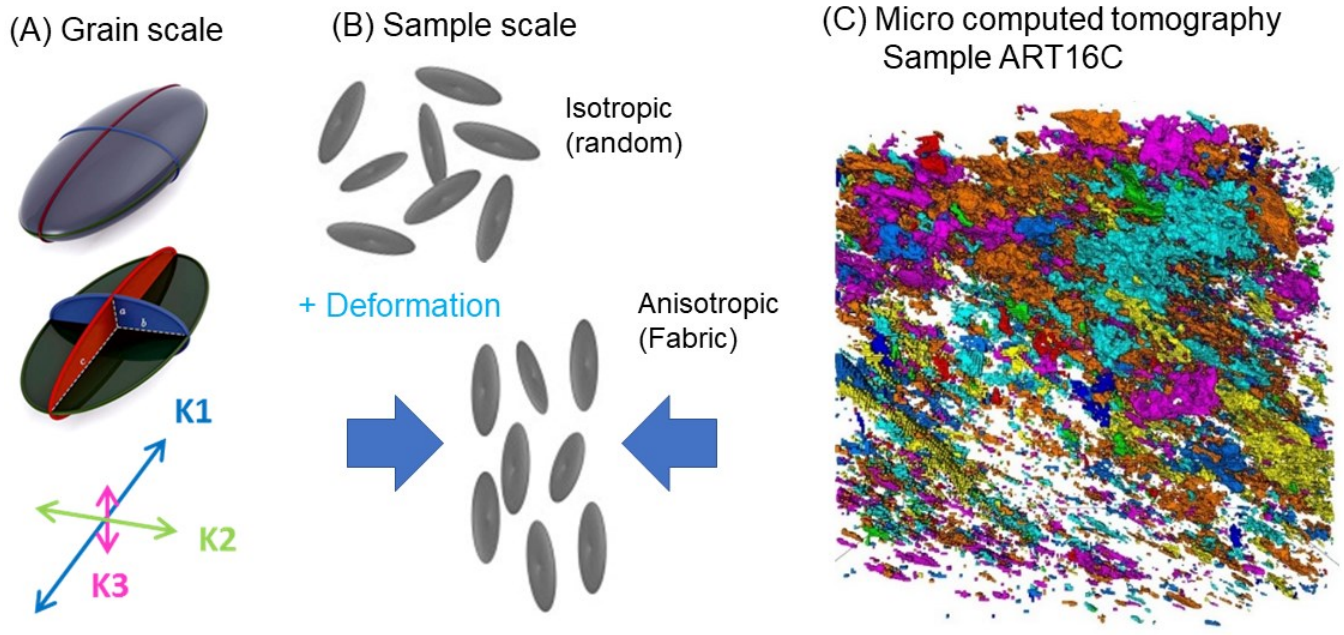

Figure 17: (A) Anisotropy of magnetic susceptibility at the grain scale corresponds to the preferred crystallographic axes of a magnetic grain referred to as K1 which represents the long axis of the grain, and the vector of maximum susceptibility), K2 (the intermediate), and K3 (the short axis). (B) Within a rock the alignment of grains determines whether that rock is isotropic or anisotropic. Isotropic rocks generally have randomly oriented grain, which collectively have no preferred alignment, whereas in anisotropic rocks the grains are preferentially aligned. (C) Grain alignment, which corresponds to the measured AMS fabric can be mapped in using micro-computed tomography (from Austin et al., 2016a).

https://doi.org/10.5194/essd-2023-464
Preprint. Discussion started: 20 February 2024

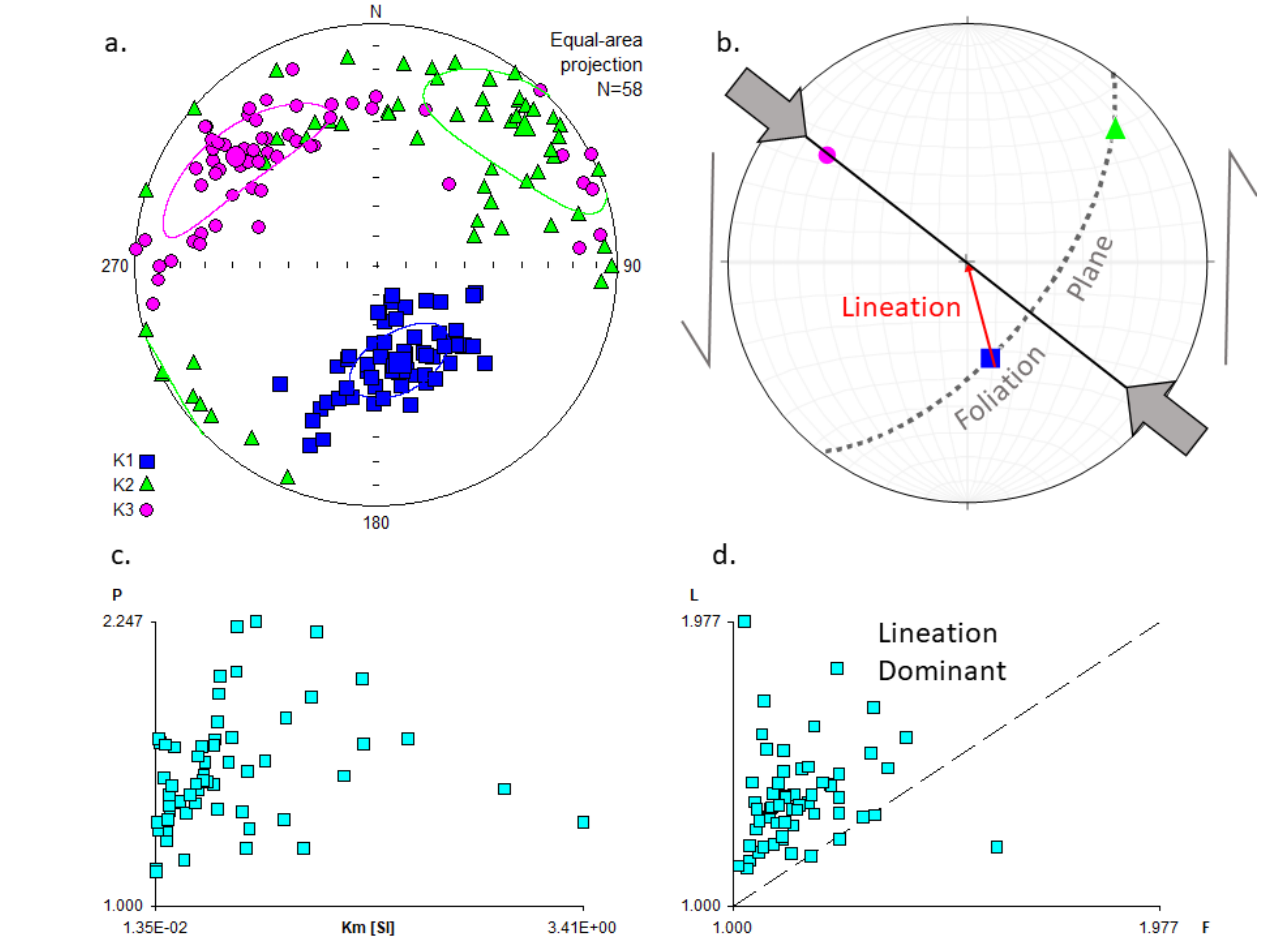

Figure 18. AMS data for samples from the Hanging Wall Shear Zone, Ernest Henry deposit. A) Stereonet in which the three AMS tensors are plotted for each specimen; B) Summary of the structural information derived from the AMS data.; C) Plot of P (anisotropy factor (K1/K3) vs magnetic susceptibility; D) Plot of L (lineation) vs F (foliation). From Austin et al., 2021b.

https://doi.org/10.5194/essd-2023-464
Preprint. Discussion started: 20 February 2024

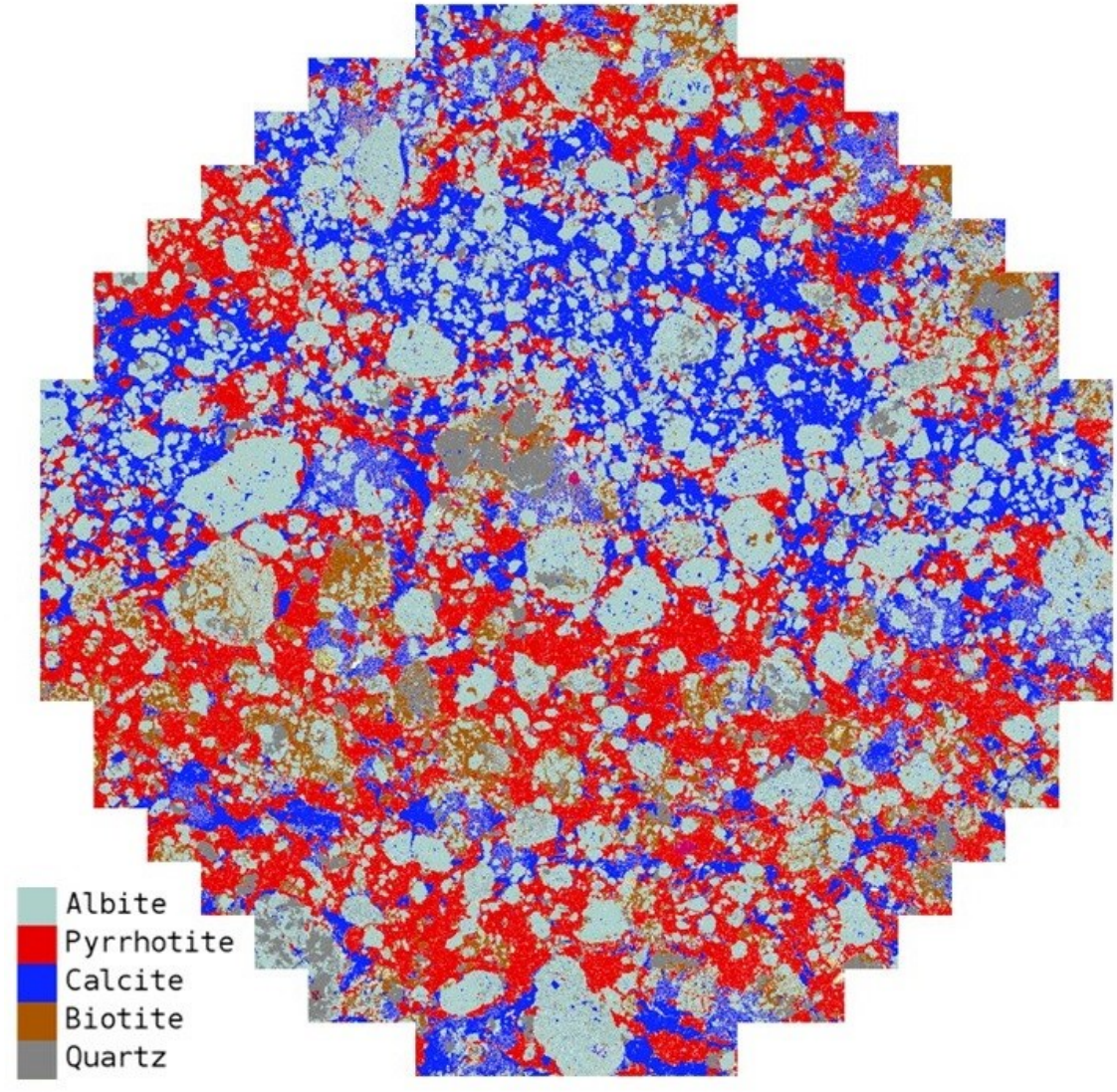

Figure 19: One of the more interesting TIMA images, sample CAN003 is a micro-breccia from Canteen prospect, with sodic altered clasts in a matrix of monoclinic (magnetic) pyrrhotite and calcite. The matrix displays classic Durchbewegung textures, which result from ductile flow in pyrrhotite which mills and rotates the breccia clasts.

https://doi.org/10.5194/essd-2023-464
Preprint. Discussion started: 20 February 2024

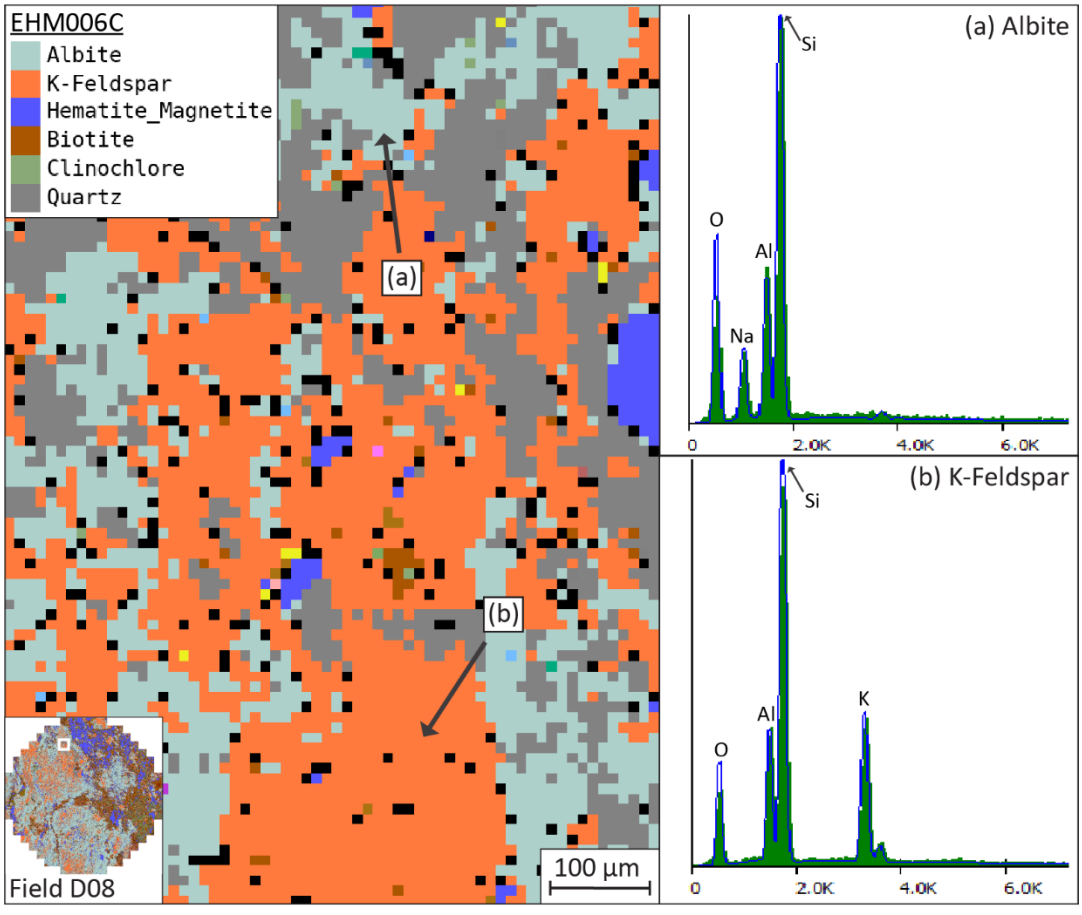

Figure 20: Mineral phase panorama from sample EHM006, Field D06, highlighting the mineral classification library at the pixel-scale and a) X-ray spectra from albite in the sample and b) X-ray spectra from K-feldspar in the sample. These minerals are constrained not only by their key elemental expression but elements that set them apart from similar phases, i.e. albite will not only be constrained by O, Na, Al and Si, but by Ca and K, to differentiate from more calcic feldspars and from K-feldspar along with other elements where overlaps may occur.

https://doi.org/10.5194/essd-2023-464
Preprint. Discussion started: 20 February 2024

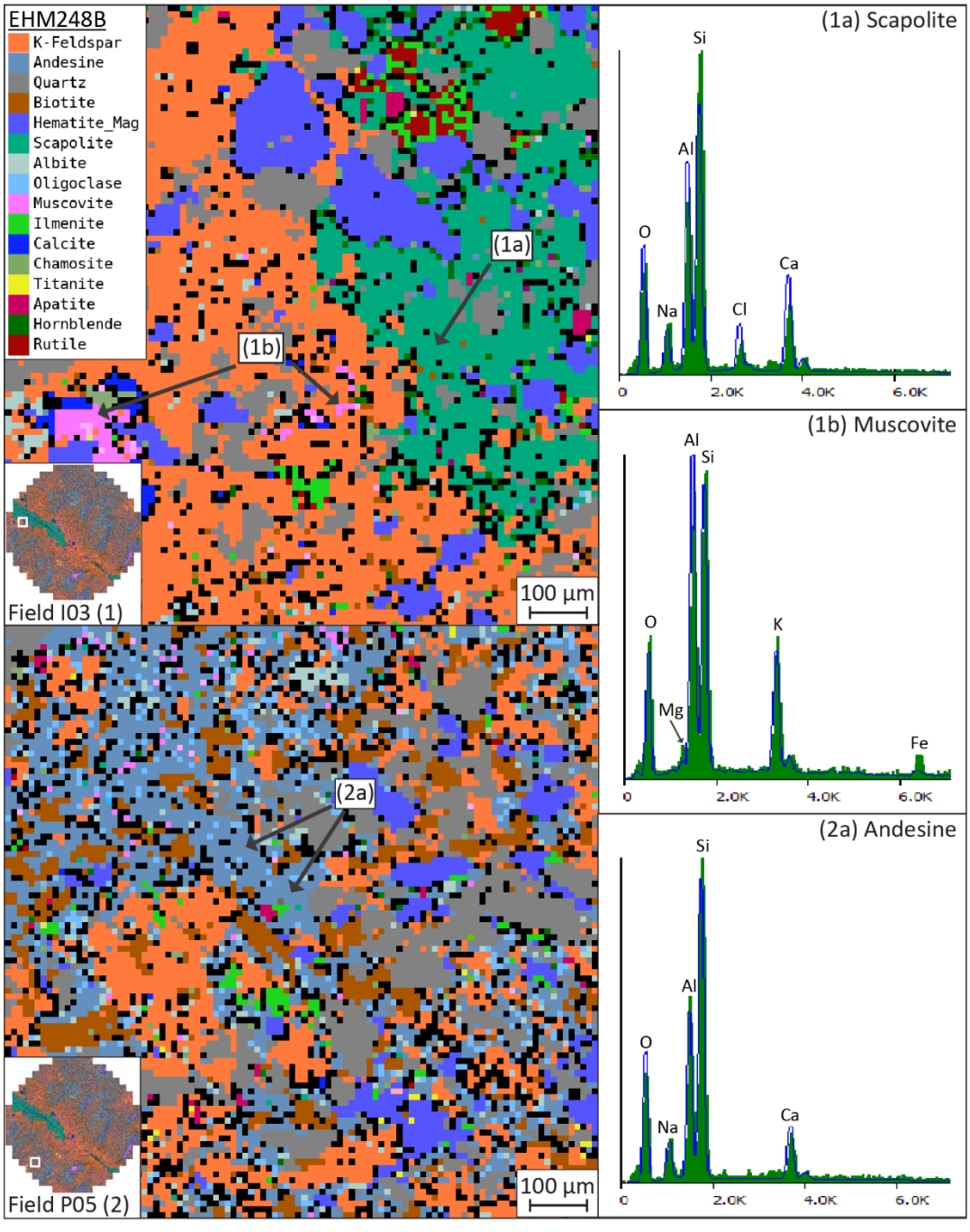

Figure 21: Mineral phase panorama from sample EHM248, Field I03 (1) and P05 (2), highlighting spectra from potentially competing mineral phases such as scapolite and andesine and alteration mineral muscovite. While the X-ray spectra from scapolite in 1a) is similar to the andesine spectra in 2a) it is able to be distinguished by adding a strict Cl constraint into both mineral classifications. 1b) The endmember composition of muscovite does not contain any Fe or Mg; however, it is a common impurity in white micas, therefore the muscovite classification has been edited to allow a small amount of Fe and Mg. After a specified limit, increases in Mg or Fe (and a decrease in Al and increase in Si) would see the phase classified as phengitic muscovite.

https://doi.org/10.5194/essd-2023-464
Preprint. Discussion started: 20 February 2024

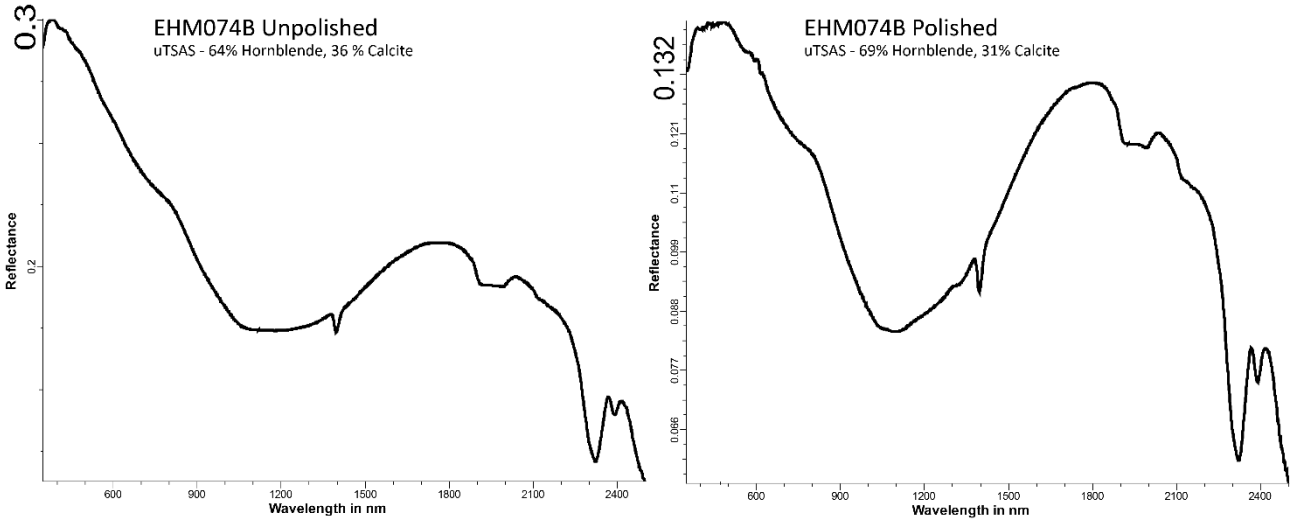

Figure 22: ASD spectra of sample EHM047B before and after polishing; notethe decrease in overall reflectance (VS albedo) in the polished sample from a max reflectance of 0.3 to 0.123 as well as the negligible change in the qualitative TSA mineralogy outputs

https://doi.org/10.5194/essd-2023-464
Preprint. Discussion started: 20 February 2024

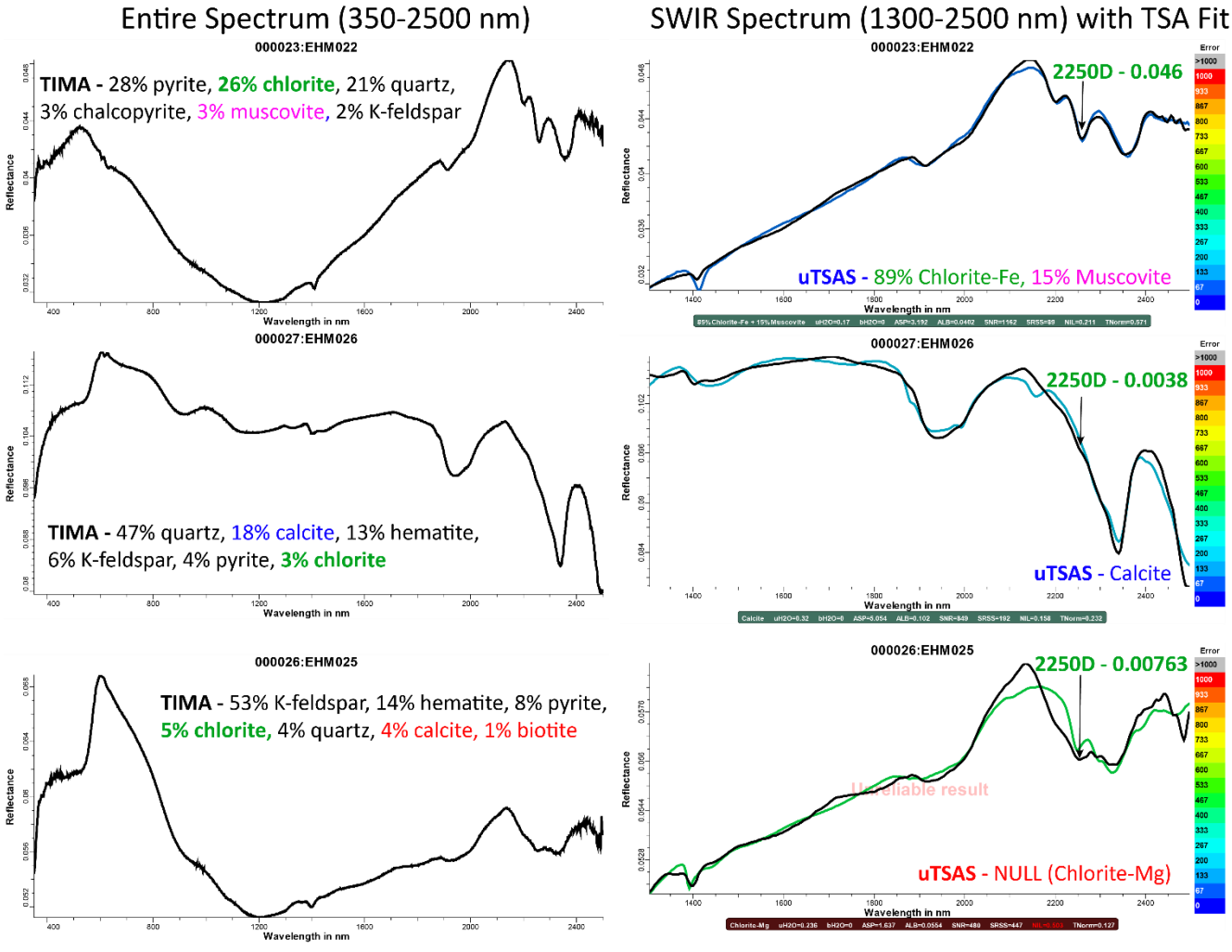

Figure 23: ASD spectra (left) and corresponding user TSA outputs and TSA modelled spectra (colored) overlain on the sample spectrum (black) for the SWIR spectral region (right) for three samples (EHM022, EHM026, EHM025). The TSA modelled spectra are coloured by error with the top sample (EHM022) having the lowest error. TIMA mineralogy results are provided for comparison as well as the output of the 2250D base scalars which approximates the abundance of chlorite (and biotite) and provides an improved proxy for chlorite abundance than the TSA results.

https://doi.org/10.5194/essd-2023-464
Preprint. Discussion started: 20 February 2024

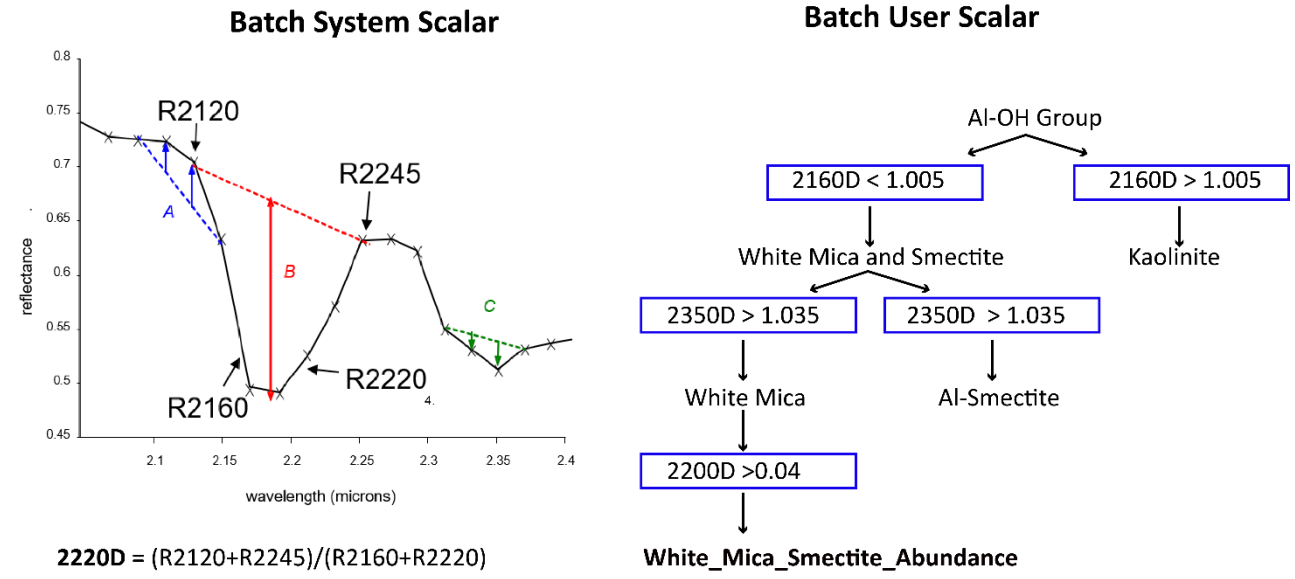

Figure 24: Schematics for derivation of the batch system 2200D scalar and the batch user White_Mica_Smectite_Abundance scalar, both of which probe the 2200 nm Al-OH spectral absorption feature.

1255

https://doi.org/10.5194/essd-2023-464
Preprint. Discussion started: 20 February 2024

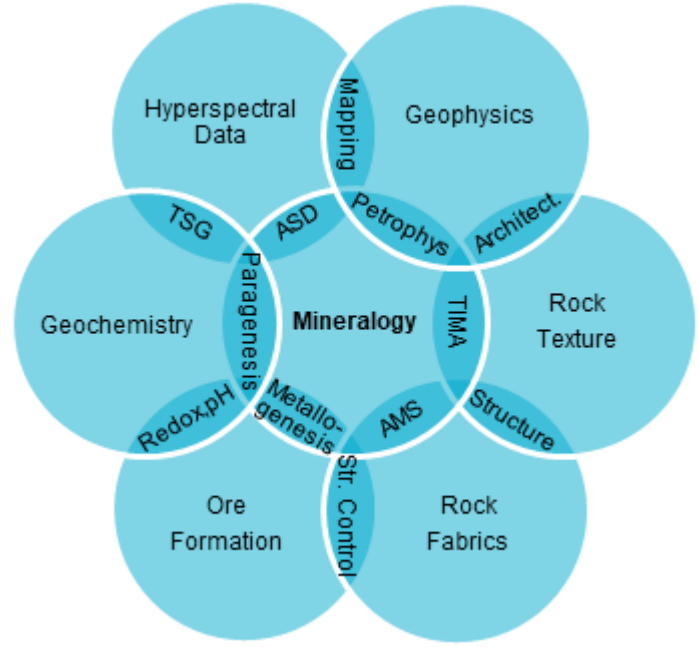

1260 **Figure 25: Venn diagram illustrating how different techniques integrate to produce scale consistent mineral systems exploration and targeting tools. Mineralogy, at the centre is the key link to all other techniques and tools and linking with the major geoscience fields. The inner areas or overlap are tools and observations we use to link mineralogy to other areas of geoscience. The outer areas of overlap are primarily where different areas of geoscience can be integrated to provide insights into the key mineral systems characteristics e.g., the five questions (Walshe, et al., 2005).**

1265

https://doi.org/10.5194/essd-2023-464
Preprint. Discussion started: 20 February 2024

Figure 26: Examples of Core-shed tools that can be used for mineral system characterisation and targeting: a portable X-ray fluorescence analyser (pXRF), portable reflectance spectrometers (ASD), magnetic susceptibility and conductivity meter and gamma-ray spectrometer.

https://doi.org/10.5194/essd-2023-464
Preprint. Discussion started: 20 February 2024

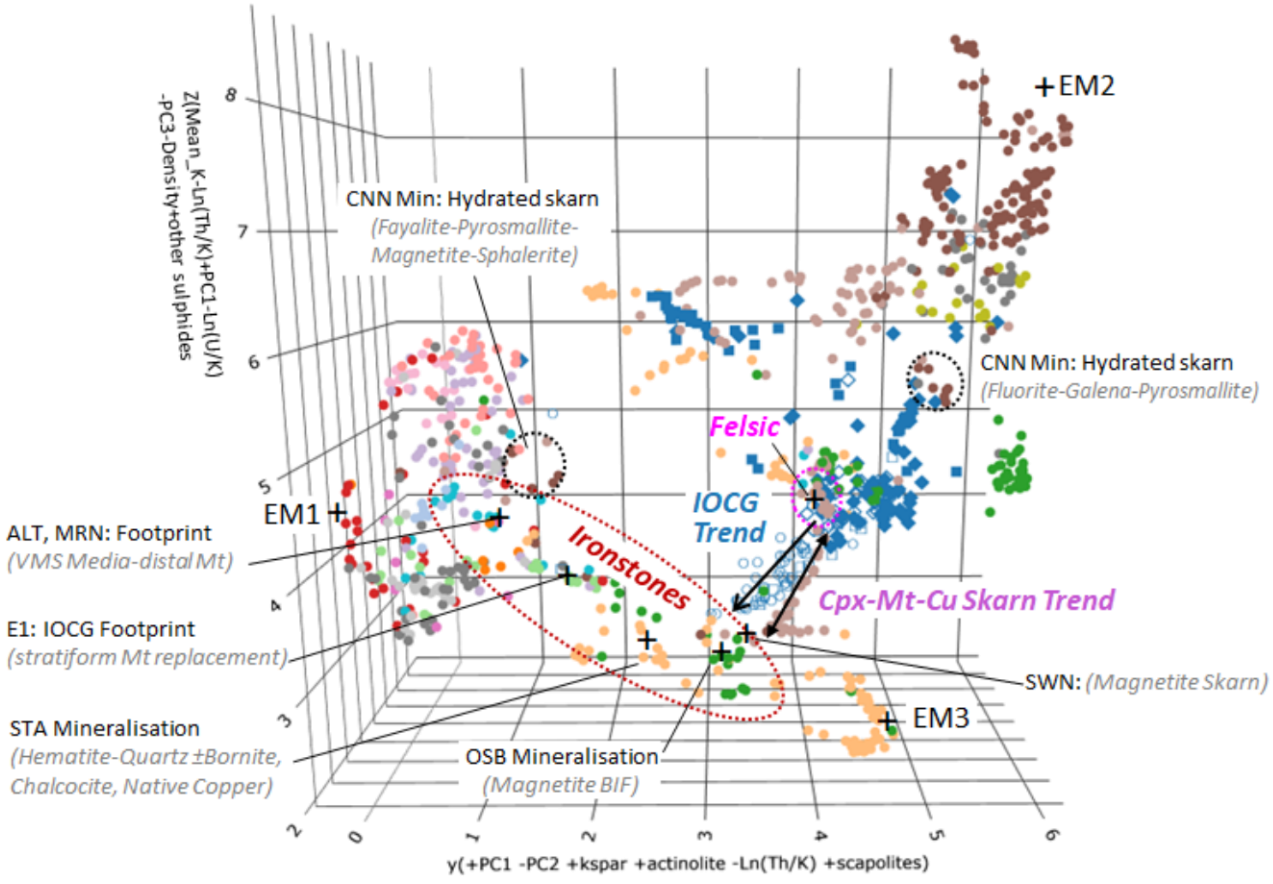

Figure 27: UMAP projection of all samples from all deposits (using only the petrophysical, mineralogical and hyperspectral properties), highlighting three main endmembers, and major intermediate host lithologies. Note that as the projection is developed from a network representation of similarities between samples, samples plotting intermediate between other identifiable groups do not necessarily exhibit precisely intermediate character (as could be concluded if plotting the original features), and rather they have similarities to both groups. However, in some cases the projection has indeed highlighted some key geological features which can be related to the projection axes (x, y, z). Figure from Williams, et al., 2022.

https://doi.org/10.5194/essd-2023-464
Preprint. Discussion started: 20 February 2024

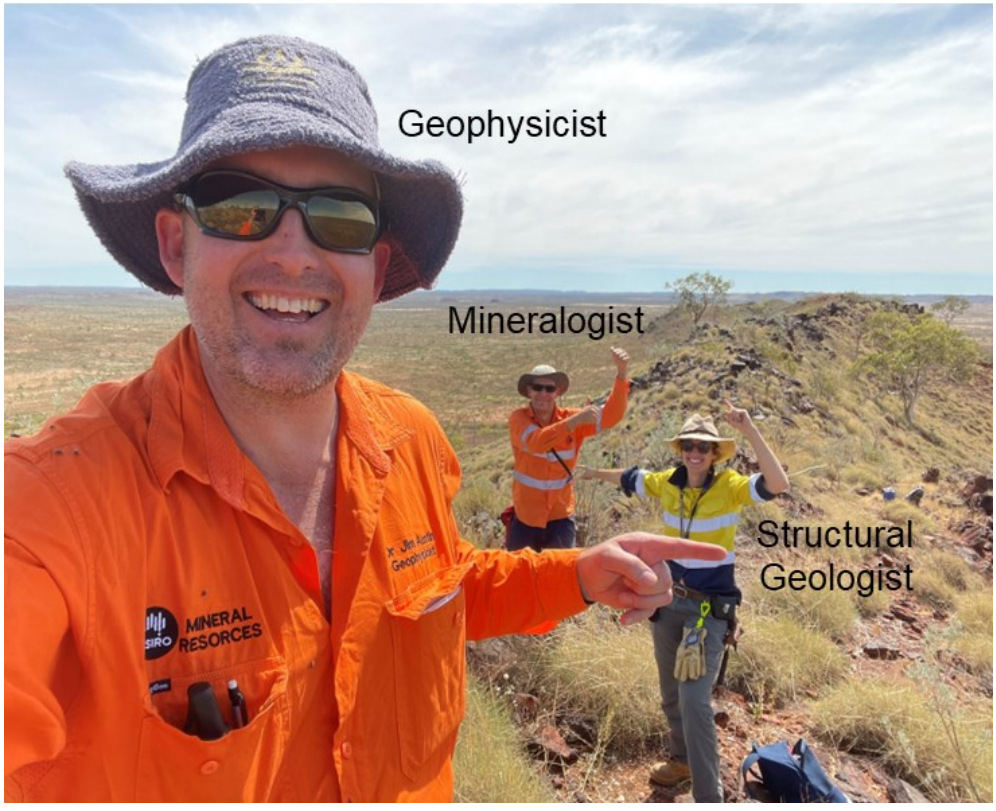

Figure 28: The integration of domain expertise is critical to understanding how different vectors to mineralisation integrate in practise. This geological understanding is critical to underpin sensible utilisation of advanced data analytics.